Dynamic response of monolithic and precast concrete joint with wet connections under impact loads

Huawei Li[1,2], Wensu Chen[2]*, Zhijie Huang[2], Hong Hao[2]*, Tuan T. Ngo[2], Thong M. Pham[2],

Kge Jack Yeoh[2]

[1]School of Civil Engineering, Guangzhou University, China

[2]School of Civil and Mechanical Engineering, Curtin University, Australia

* Corresponding authors:

wensu.chen@curtin.edu.au (W. Chen), hong.hao@curtin.edu.au (H. Hao)

Abstract: Precast concrete (PC) structures have been popularly used in construction practice and PC beam-column joints are critical for structural integrity and safety. In this study, dynamic responses of one monolithic reinforced concrete (RC) joint and three PC joints with different wet connection configurations were investigated by using a pendulum impact test system. The impact behaviours of monolithic RC and PC joints were examined and compared in terms of failure modes, dynamic responses, and energy dissipation. The effects of various wet connection configurations on the dynamic response of PC joints were discussed and analysed. It is found that the interface damage between PC beam and joint led to the reduced integrity of the PC joints. In addition, numerical models of beam-column joints were developed by using software LS-DYNA and calibrated by the test data. The calibrated numerical model was used to investigate the influences of various wet joint configurations on its performance subjected to impact at different locations. Numerical results showed that the shear key and interface rebar employed for wet connections were beneficial to resist shear-governed damage but less effective in resisting flexural-governed damage induced by impact loads. Therefore, the wet connections should be properly designed for PC joint to resist the designated impact loading

25   scenarios.

26   **Keywords:** Precast concrete; Beam-column joint; Wet connection; Dynamic response; Impact

27   load

28   **1. Introduction**

29   In recent years, precast concrete (PC) structures have been extensively employed in

30   residential, commercial, and industrial constructions [1-3]. The PC construction techniques can

31   improve construction quality, speed up construction process, and reduce on-site waste and labor

32   cost. The PC components prefabricated in factories are assembled onsite with various

33   connections. ACI 550.2R-13 classifies common connections into the wet connection and dry

34   connection [4]. Currently, PC joints with wet connections are widely used in PC structures since

35   they exhibit a similar capacity to conventional monolithic reinforced concrete (RC) joints

36   through the emulative design method [5-7]. With regard to wet connections, various connecting

37   techniques such as grouted sleeve [8, 9], lap-splice [10, 11], and 90° bend [1, 12, 13], are

38   employed to ensure the continuity of longitudinal rebars inside PC beams and columns. In

39   addition, the interface of PC components is usually roughened in advance to increase the bond

40   strength between PC and cast-in-place concrete (CIPC) components [7, 12]. Moreover, shear

41   keys [11, 14, 15] and additional interface rebars through interfaces [6, 13] could also enhance

42   the bonding between PC and CIPC components.

43   PC beam-column joints with wet connections, connecting the PC beams and columns, are

44   the key components for the integrity of frame structures. They should be designed to have

45   sufficient capacity to transfer bending moment, shear force, and axial force under static and

46   dynamic loads. The poor design of wet connection would cause the premature failure of PC

47   beam-column joints [16]. The performances of PC beam-column joints with wet connections

48   under cyclic loading [2, 8, 17] and static pushdown loading [18, 19] have been investigated in

49 the previous studies. It is found that the failure modes of PC joints with wet connections were

50 different from those of monolithic RC joints. The wet connections between PC and CIPC

51 components were prone to crack owing to the discontinuity of concrete [20]. The cracks might

52 initiate and spread intensively at the interface between the PC and CIPC components in PC

53 joints, while the concrete cracks were more evenly distributed in the plastic zone and the core

54 area of beam-column joint in monolithic RC joints. These different failure modes of PC and RC

55 joints are mainly resulted from the connection configurations, i.e., longitudinal rebar connecting

56 types and the interfaces between the PC and CIPC components. Since the interfaces are deemed

57 the weakest part of the PC joints, the interface is usually roughened with different roughness to

58 improve the bonding between PC and CIPC components and meet with design requirements

59 [12, 21, 22]. Moreover, additional reinforcement at interface could be employed to mitigate the

60 cracks along the interface [6, 13]. Since the wet connection configurations are key factors

61 affecting the load-carrying capacity of PC joints, appropriate design of wet connections should

62 be employed in the PC structures to resist various loading scenarios.
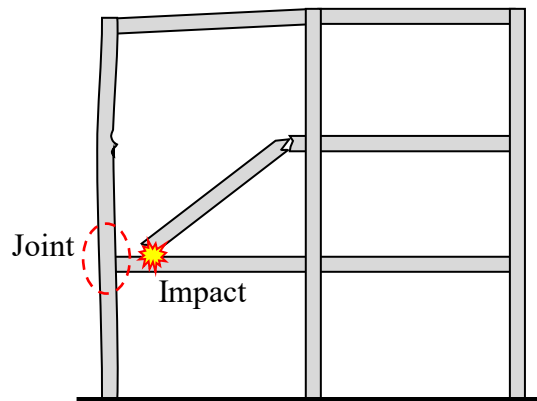
63
64 Fig. 1. Falling component impacts on the joint area.

65   In addition to seismic loading, PC structures might suffer extreme loadings such as blast

66 and impact. As shown in Fig. 1, failed components induced by extreme events from the upper

67 floor might impact and cause damage to the lower floor and even progressive collapse, which

68 depends on the performance of joint under impact [23, 24]. To date, the impact behaviour of

69 RC and PC beams under impact has been investigated experimentally, numerically, and

70 analytically [20, 25-29]. It is well known that the stress wave induced by impact loads would

71 propagate from the impact location to the beam ends [30-32]. In real frame structures, the beam

72 ends are constrained by joint areas through various connections. Therefore, the stress waves

73 induced by impact loading caused by falling components as shown in Fig. 1 may generate

74 damage at the joint areas. If the joint at the lower floor could resist the damage generated by

75 the impact loading, the progressive collapse of frame structures could be avoided [33, 34].

76 Although the impact behaviours of steel joint and steel-concrete composite joint have been

77 experimentally and numerically studied [23, 24, 35-37], the investigations on the dynamic

78 response of PC joint with wet connection have not been reported in the open literature.

79 Therefore, it is essential to examine the dynamic response and impact performance of PC beam-

80 column joints with various wet connection configurations under impact loads.

81 In this study, the monolithic RC joint and the PC joints with different wet connection

82 configurations were tested by using a pendulum impact testing system. The impact behaviours

83 of joints were studied and analysed in terms of failure mode, impact force, displacement

84 response, and energy dissipation. The effects of shear key and interface rebar along the interface

85 between PC and cast-in-place concrete (CIPC) components on the impact behaviour of joints

86 were investigated. In addition, numerical models of joints were developed in LS-DYNA and

87 calibrated by using the test results. With the calibrated numerical model, the performances of

88 beam-column joints were further investigated to study the effects of different wet connection

89 configurations and impact locations on the dynamic response characteristics and damage

90 mechanisms of PC joints.

91 **2. Experimental program**

92 **2.1. Specimen design**

93 In order to investigate the impact behaviour of beam-column joints, four exterior beam-

These specimens had the same dimensions but

the connection configurations at the joint area were different. The dimensions of beam and

column sections were 200 mm × 150 mm and 200 mm × 200 mm, respectively. A total of four

longitudinal rebars with a diameter of 16 mm were used for the beam and column. The

longitudinal rebars in beam were terminated with a 90° bend and the anchorage lengths for top

and bottom longitudinal rebars were 100 mm and 80 mm respectively in the joint area to ensure

sufficient anchorage. The stirrups with a diameter of 10 mm had a space of 70 mm along the

beam and column except the joint area in which the space was reduced to 50 mm. Specimen

MCJ was a monolithic RC joint as shown in Fig. 2(a), in which the whole column with a length

of 1280 mm and the beam with a length of 800 mm were cast at the same time to form a

monolithic joint.

(a) MCJ   (b) PCJ

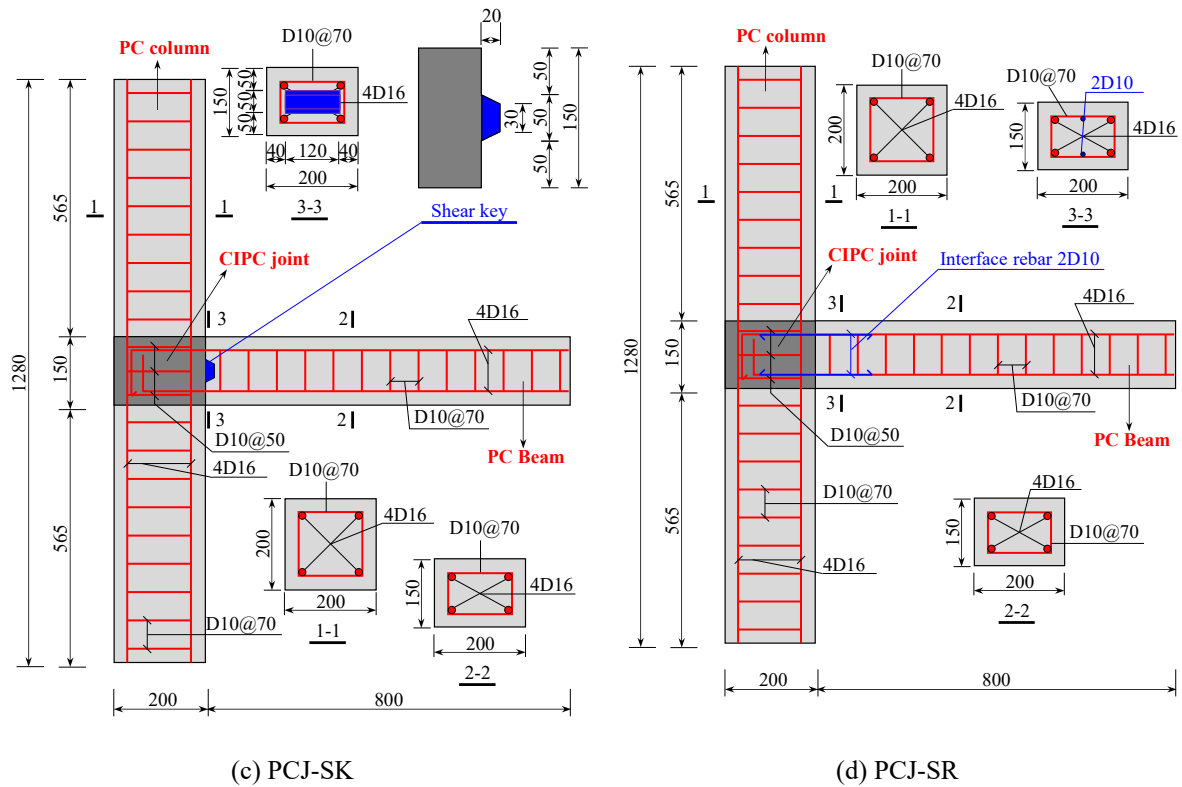(c) PCJ-SK   (d) PCJ-SR
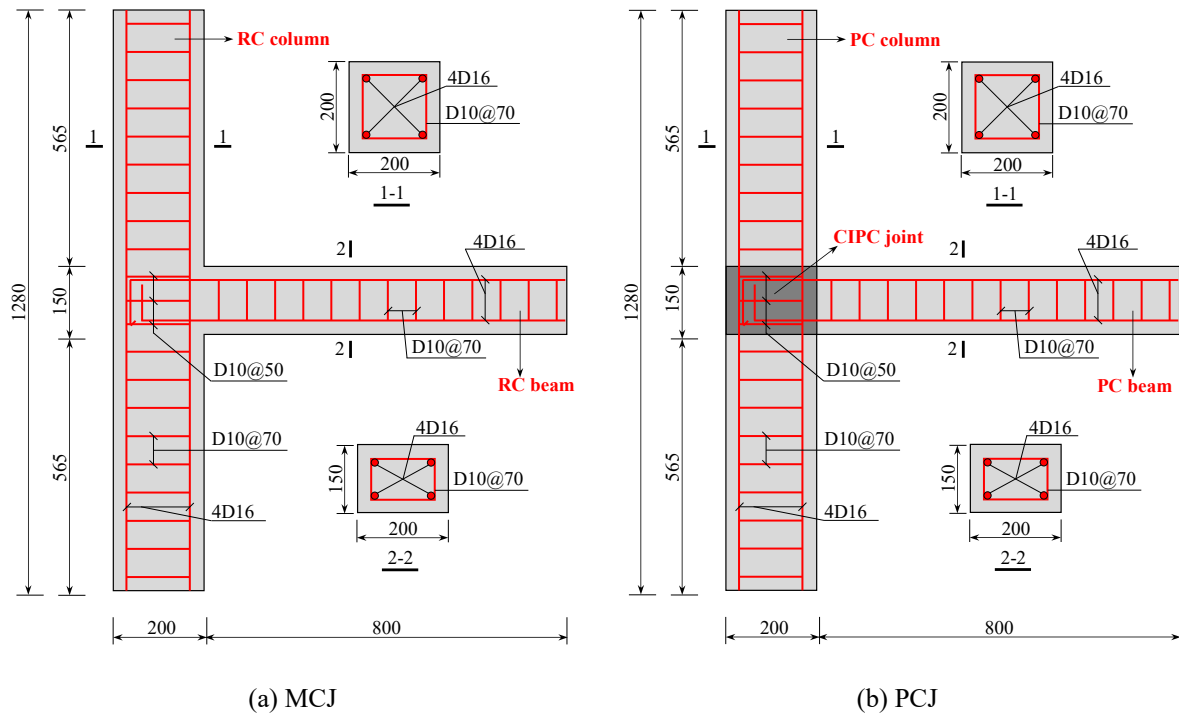
Fig. 2. Dimension and configuration of tested joint specimens.

108   For other three PC joint specimens named PCJ, PCJ-SK, and PCJ-SR, the PC beam and

109   two PC columns were cast first. After the curing of PC beam and columns, the joint areas were

110   filled with CIPC to assemble the PC beam and columns as shown in Fig. 3. The surfaces of PC

111   beam and columns toward the joint area were roughened before casting the joint component to

112   ensure the integrity between PC and CIPC for all the PC joints as shown in Fig.4. Moreover, a

113   trapezoidal shear key as presented in Fig. 4 was designed at the interface of PC beam for

114   specimen PCJ-SK. The dimension of shear key is illustrated in Fig. 2(c). For specimen PCJ-SR,

115   longitudinal interface rebars with a length of 250 mm and a diameter of 10 mm through the

116   interface between PC and CIPC were placed at the top and bottom sides of the PC beam and

117   joint area (2D10 labelled in section 3-3 as shown in Fig. 2(d)) to increase the integrity of

118   interface. The average concrete compressive strength for specimen MCJ and the precast beams

119   and columns of the PC specimens was 64.75 MPa and that of CIPC joint area was 68.34 MPa

120   at 28-day. It is noted that the concrete compressive strength of CIPC joint area should be slightly

6

121 higher than that of PC components as required in Refs. [4, 16]. The nominal yield strength of

122 the longitudinal steel rebars and stirrups was 500 MPa.
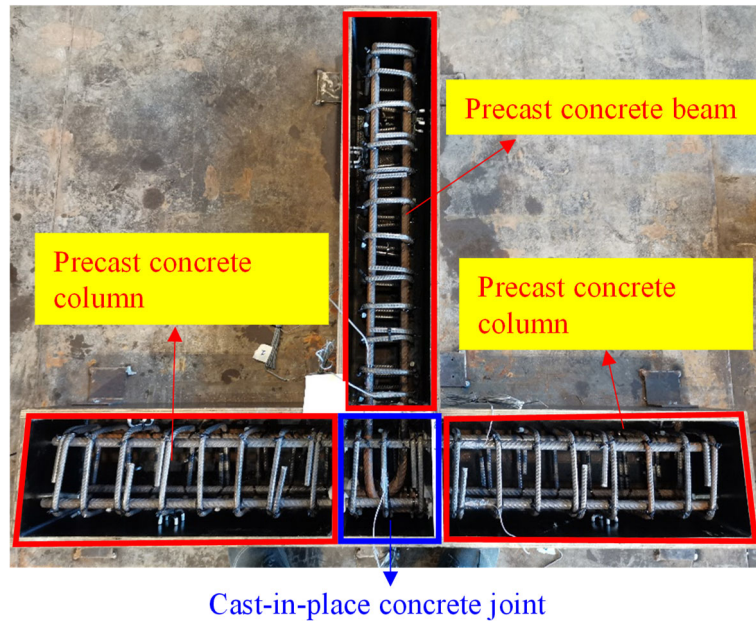
123
124 Fig. 3. Construction of PC joint with wet connection.
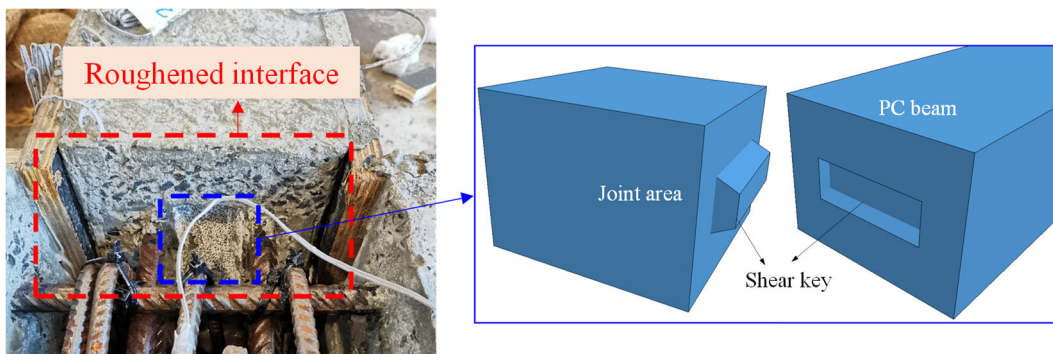
125
126 Fig.4. Roughened interface and shear key.

127 **2.2. Test setup and instrumentation**

128 The impact test was carried out by using a pendulum impact testing system as shown in

129 Fig. 5. A 550 kg impactor consisting of load cell and steel blocks was connected to a steel arm

130 with a length of 2.24 m. The top of the steel arm was hinged on a rigid reaction frame. The

131 impactor was lifted to a designated angle θ that was measured by an inclinometer attached to

132 the steel arm and then released to impact the beam. A load cell with a capacity of 500 kN was

133 installed in front of the impactor to measure the impact force acting on the beam with a sampling

134 rate of 50 kHz. The impact head was made of a steel cylinder with a diameter of 50 mm. The

column of joint specimen was hinge supported horizontally by the rigid reaction frame and

vertically by the strong floor. The distance between the two hinge supports was 1030 mm as

shown in Fig. 5(a). A hydraulic jack placed horizontally applied an axial force of 60 kN (about

2% of the column capacity) onto the column to constrain the horizontal movement of specimen

in the test [39]. A high-speed camera with a sampling rate of 20,000 frames per second was

employed to record the entire impact process. The tracking point at the impact location enabled

the high-speed camera to capture the time history of displacement at the impact location by

using the digital image correlation (DIC) technique. By considering the capacity of tested

specimens and the pendulum impact test apparatus, each specimen was impacted four times.

The release angle (θ) of impactor, the corresponding designed impact velocity, and the actual

impact velocity for each impact are summarized in Table 1. In the first impact, the impactor

with a mass of 550 kg and a designed impact velocity of 2.42 m/s struck the specimen. This

impact could cause appreciable specimen damage without causing specimen failure. Then the

designed impact velocity increased to 3.21 m/s in the second to the fourth impact to obtain more

severe specimen damage. Each specimen was impacted four times until the specimen failure.

Table 1. Summary of impact scenarios.

Specimen	Impact No.	Release angle (°)	Designed impact energy E_k(J)	Designed impact velocity (m/s)	Actual impact velocity (m/s)
MCJ	1	30	1610.51	2.42	2.33
	2	40	2833.63	3.21	3.11
	3	40	2833.63	3.21	3.19
	4	40	2833.63	3.21	3.15
PCJ	1	30	1610.51	2.42	2.28
	2	40	2833.63	3.21	3.16
	3	40	2833.63	3.21	3.03
	4	40	2833.63	3.21	3.06
PCJ-SK	1	30	1610.51	2.42	2.30
	2	40	2833.63	3.21	3.06
	3	40	2833.63	3.21	3.11
	4	40	2833.63	3.21	3.16
PCJ-SR	1	30	1610.51	2.42	2.39
	2	40	2833.63	3.21	3.21
	3	40	2833.63	3.21	3.09
	4	40	2833.63	3.21	3.12
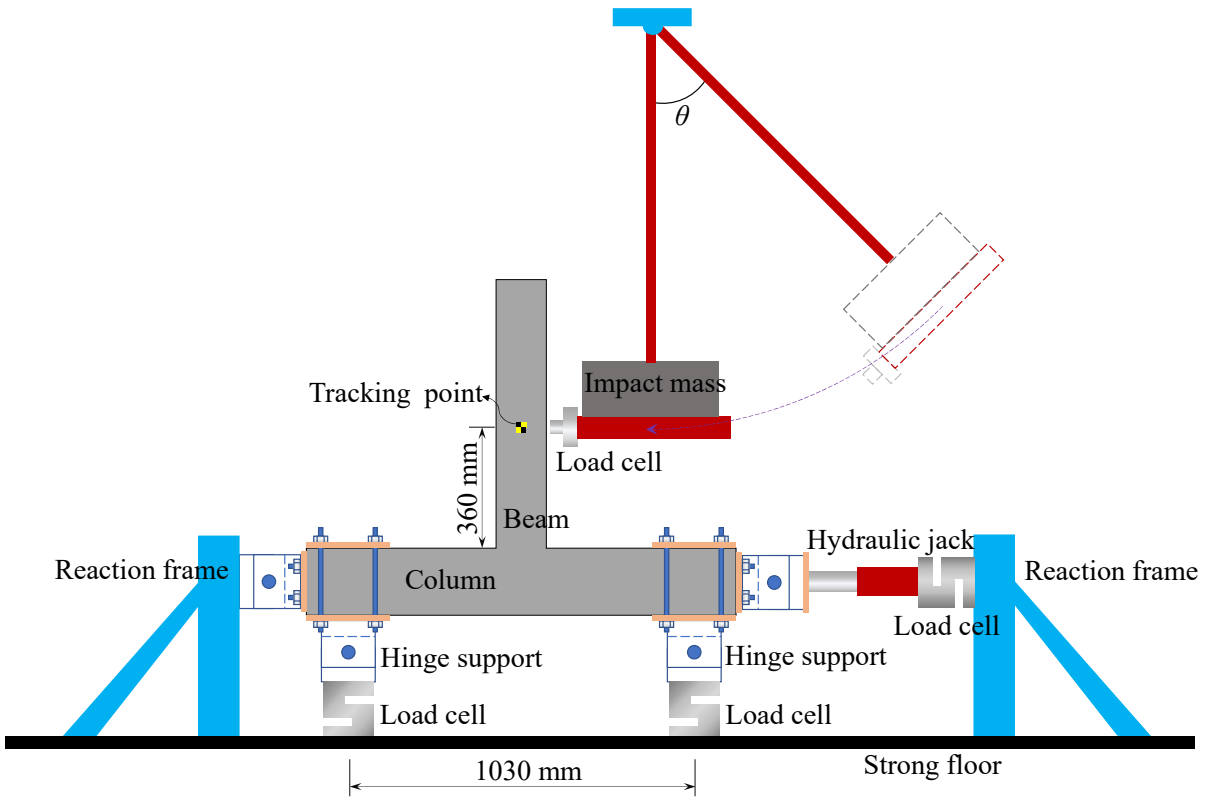
(a) Schematic diagram of test setup
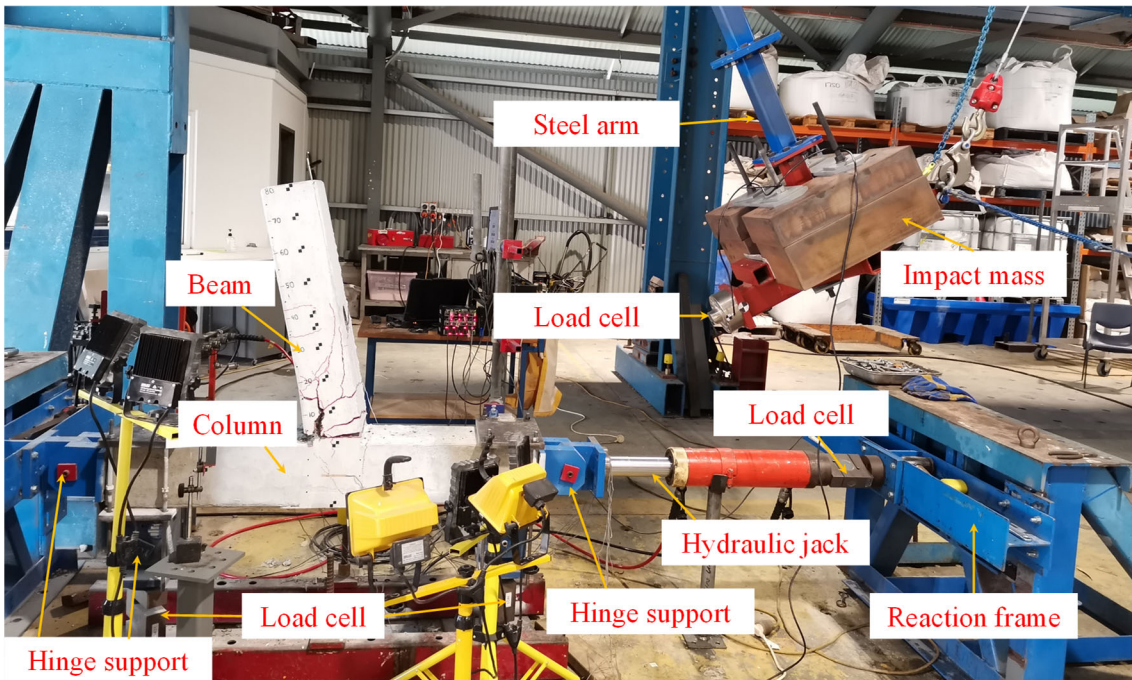
(b) Photograph of test setup

Fig. 5. Pendulum impact test setup.

3. Experimental results and discussion

Test results of the four beam-column joints with different wet connection configurations subjected to impact loads are presented and analysed in this section to discuss their effects on the dynamic performance of the joints. The impact force, displacement, and dissipated energy of the specimens are summarized in Table 2.

Table 2. Test results of specimens.

Specimen	Impact No.	Peak impact force (kN)	Maximum displacement (mm)	Residual displacement (mm)	Dissipated plastic energy (J)	Energy dissipation ratio (E_p/E_k)
MCJ	1	213.57	13.41	2.87	604.06	0.38
	2	243.37	23.21	8.14	1367.66	0.48
	3	221.50	30.56	16.15	1757.71	0.62
	4	202.86	37.02	19.49	2053.78	0.72
PCJ	1	-	14.05	2.63	-	-
	2	249.57	25.42	8.65	1411.85	0.50
	3	223.20	35.74	19.47	2130.88	0.75
	4	177.21	40.30	20.10	2080.38	0.73
PCJ-SK	1	214.28	16.91	3.16	954.48	0.59
	2	270.23	29.07	13.67	2010.58	0.71
	3	216.50	39.28	23.67	2291.43	0.81
	4	169.38	45.00	26.63	2185.51	0.77
PCJ-SR	1	212.33	14.54	2.68	674.41	0.42
	2	274.55	25.40	10.90	1671.29	0.59
	3	245.49	35.42	17.66	2114.81	0.75
	4	202.52	39.30	20.30	2113.88	0.75

Note: "-" means the data was not recorded due to the malfunction of data acquisition system. Initial kinetic energy (E_k); Dissipated plastic energy (E_p).

3.1. Failure mode

Failure modes of the beam-column joints with different wet connections were compared after each impact as shown in Fig. 6. It is worth noting that the impact load was applied onto the right side of beam at the middle as illustrated in Fig. 5. Under the first impact, concrete cracks at the middle of the beams were initiated on the left side and then extended to the right side for all the specimens at the early stage of impact due to the positive bending moment induced by the impact load. This phenomenon was similar to the damage mode of beams under impact because the boundary condition of the beams had a negligible effect on the behaviour of beam at the very early stage of impact [29, 42]. With stress waves propagating from the

169   impact location to the joint area, concrete cracks were observed at the beam-to-joint interface.

170   Specimen PCJ experienced concrete cracking through the entire horizontal interface, which

171   indicates more severe interface damage than specimens MCJ, PCJ-SK, and PCJ-SR. Because

172   of shear key at the interface of specimen PCJ-SK, partial interface damage was observed at the

173   right side of interface. Moreover, the interface rebars improved integrity of the interface in

174   specimen PCJ-SR and thus resulted in uneven cracks along the interface. In addition, several

175   tensile concrete cracks on the beam close to the joint area appeared at the right side of the beam

176   and then extended to the left owing to the positive bending moment.

177   When subjected to the second impact as shown in Fig. 6(b), the existing concrete cracks

178   generated from the first impact became wider. Concrete crushing occurred at the left bottom

179   corner of the beam. Due to larger deflection of the beam, the interface damage became more

180   severe in the PC joints PCJ, PCJ-SK, and PCJ-SR. Besides, concrete cracks appeared at the

181   bottom of the left interface between the left PC column and the CIPC joint area in specimens

182   PCJ and PCJ-SR as highlighted in Fig. 6(b) because of tensile stress experienced in this area.

183   However, no concrete crack appeared at the same location for specimen PCJ-SK due to more

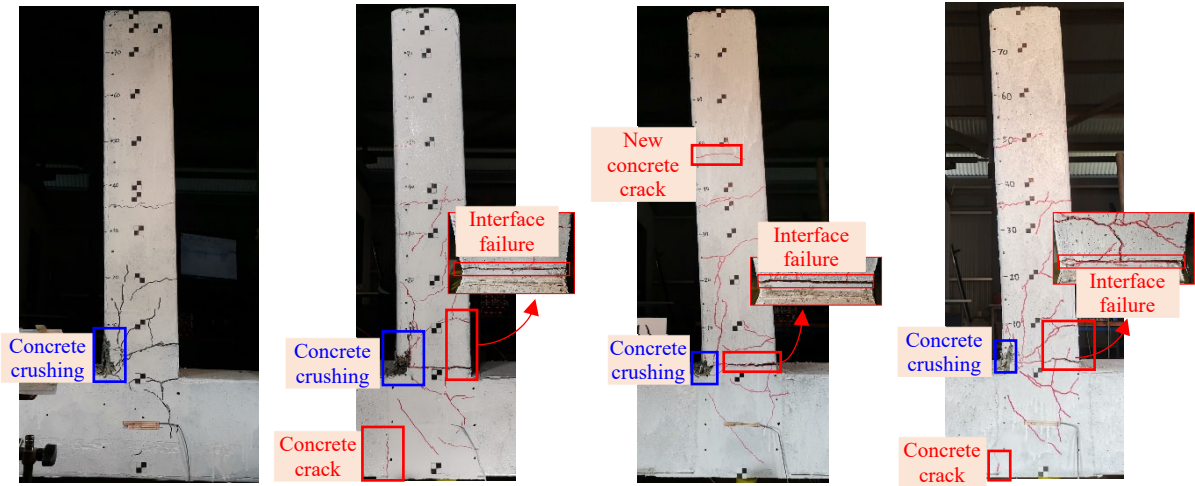184   energy dissipated by the damage of interface between PC beam and CIPC joint area.

185   The failure modes of specimens after the third impact are illustrated in Fig. 6(c). Concrete

186   at the left bottom corner of beam was crushed severely in all the specimens. The interface

187   damage between PC beam and CIPC joint area extended from the right side to the left side in

188   all the PC joints. In addition, inclined concrete shear cracks extending from the impact area

189   were observed on the PC beams of specimens PCJ, PCJ-SK, and PCJ-SR. More severe concrete

190   cracks owing to the positive bending moment on the right side of beam close to the connections

191   appeared in specimens PCJ and PCJ-SR, while PCJ-SK suffered less concrete damage in these

192   areas. This is because the right bottom corner of the PC beam in specimen PCJ-SK was lifted

193   with larger displacement after damage of the interface between the PC beam and column then

194   the PC beam at the right bottom corner experienced less constraint.
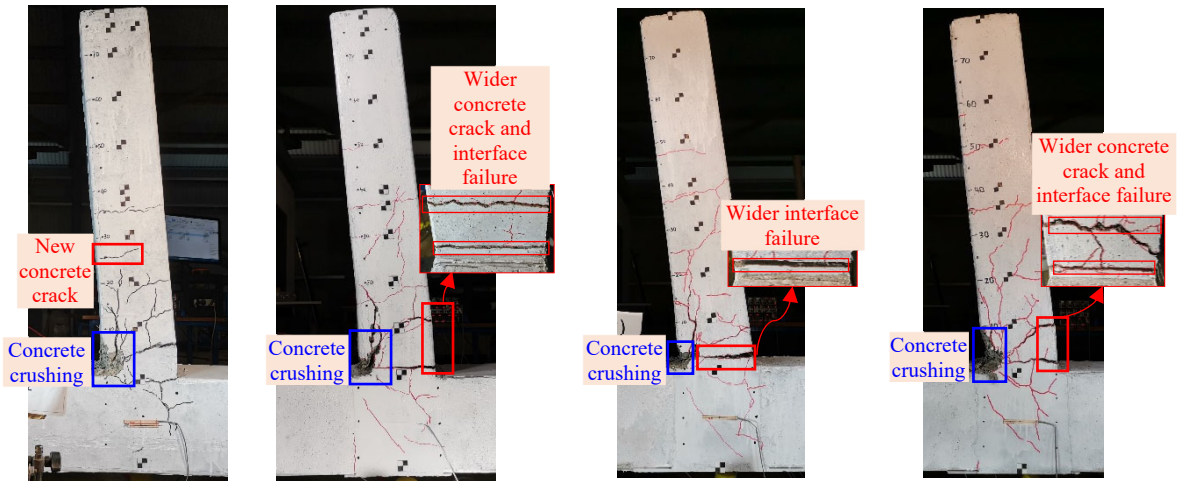
195   When subjected to the fourth impact as shown in Fig. 6(d), the specimens deflected

196   significantly and more severe concrete crushing was observed. The concrete crushing in

197   specimens MCJ, PCJ, and PCJ-SK became more severe than that in specimen PCJ-SR.

198   Moreover, specimens MCJ, PCJ, and PCJ-SR suffered more severe concrete damage on the

199   right side of the beam close to the connection than specimen PCJ-SK. Concrete damage on the

200   right side of the PC beams even caused the exposure of stirrups in specimens PCJ and PCJ-SR.

201   For specimen PCJ-SK, the PC beam rotated around the shear key after the interface damage

202   between beam and CIPC joint area, less flexural and shear cracks were observed on the PC

203   beam. In addition, all PC joint specimens experienced concrete cracks at the left interface

204   between the left PC column and CIPC joint area as highlighted in Fig. 6(d) due to the weak

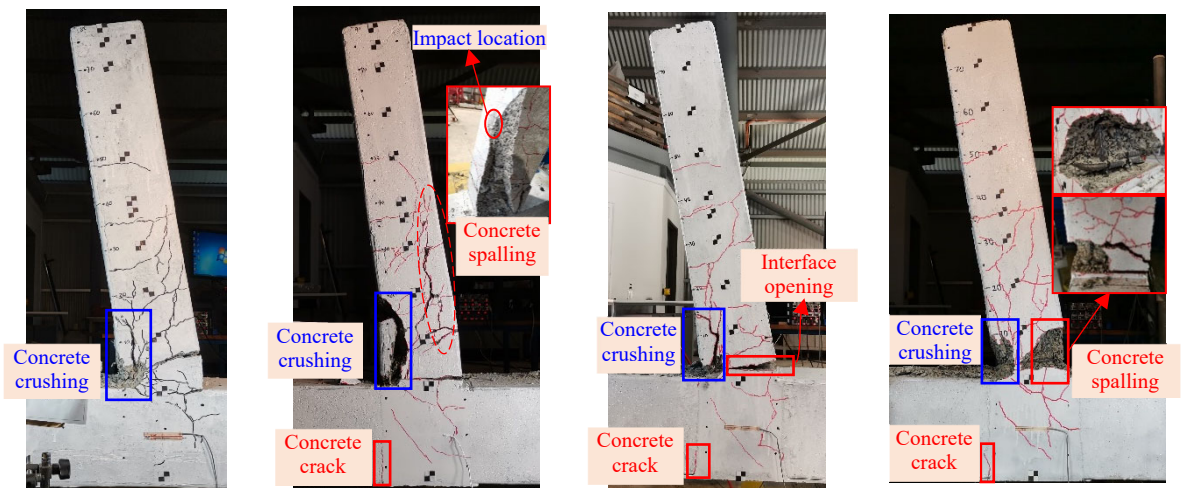205   bonding of wet interface for PC joint and the tensile stress induced by impact loads.

MCJ   PCJ   PCJ-SK   PCJ-SR

Entire interface failure

Partial interface failure

Shear cracks at joint area
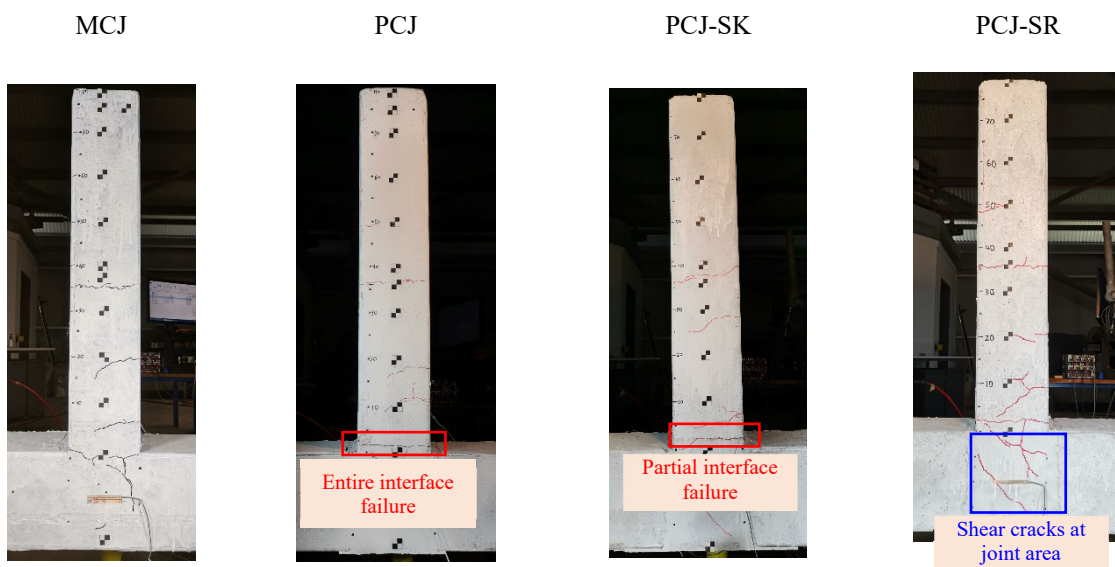
(a) 1st impact

(b) 2nd impact

(c) 3rd impact

(d) 4th impact

Fig. 6. Failure modes of joint specimens after four impacts.

3.2. Impact force

The impact force time histories of the tested specimens under four impacts are shown in Fig. 7. All the impact force profiles consisted of a primary impulse followed by a force plateau, which was caused by the interaction between the impactor and the specimen. The steel impactor impacted the beam at the initial stage and then moved together with the beam during the force plateau stage. The peak impact forces for each specimen under each impact are compared in Fig. 8. The peak impact forces of MCJ under four impacts were 213.57 kN, 243.37 kN, 221.50 kN, and 202.86 kN as listed in Table 2. The designed impact velocity of the first impact was 2.42 m/s, while the other impacts had the designed velocity of 3.21 m/s as listed in Table 1. The higher impact velocity in the second impact caused a higher peak impact force than that in the first impact. However, the peak impact force decreased gradually after the second impact to the fourth impact although the designed impact velocity was the same. The impacts caused local damage at the impact zone and thus a decrease of the contact stiffness, which led to the lower peak impact force in the subsequent impacts. In addition, the inclined impact angle between impactor and beam due to residual deflection of the beam from prior impacts resulted in a reduced contact area as illustrated in Fig. 9, which could also lead to a lower peak impact force [20, 43]. Therefore, the accumulative local damage at the impact zone and the inclined impact angle between the load cell and beam reduced the contact area and contact stiffness and thus led to a lower peak impact force in the subsequent impacts. Besides, the peak impact forces of specimens MCJ, PCJ-SK, and PCJ-SR under the first impact were 213.57 kN, 214.28 kN, and 212.33 kN, respectively, which were comparable as shown in Fig. 8, owing to the similar impact energy and contact stiffness at the impact zone. It should be mentioned that the impact force of specimen PCJ under the first impact was not recorded due to the malfunction of the data acquisition system. From the second impact to the fourth impact with the similar impact velocity, the peak impact forces of the tested specimens were different due to the initial impact angle and

231 various contact stiffness at the impact zone. In addition, the duration of primary impulse was

232 comparable for the tested specimens under four impacts as shown in Fig. 7. However, the total

233 impact duration increased with the subsequent impacts. For example, the total impact duration

234 of PCJ-SR under four impacts was 34.82 ms, 38.12 ms, 43.60 ms, and 48.52 ms, respectively.

235 This is because the accumulative impact energy caused more severe damage of specimens and

236 thus led to the decrease of global stiffness of specimen, which resulted in the increase of total

237 impact duration.

(a) MCJ
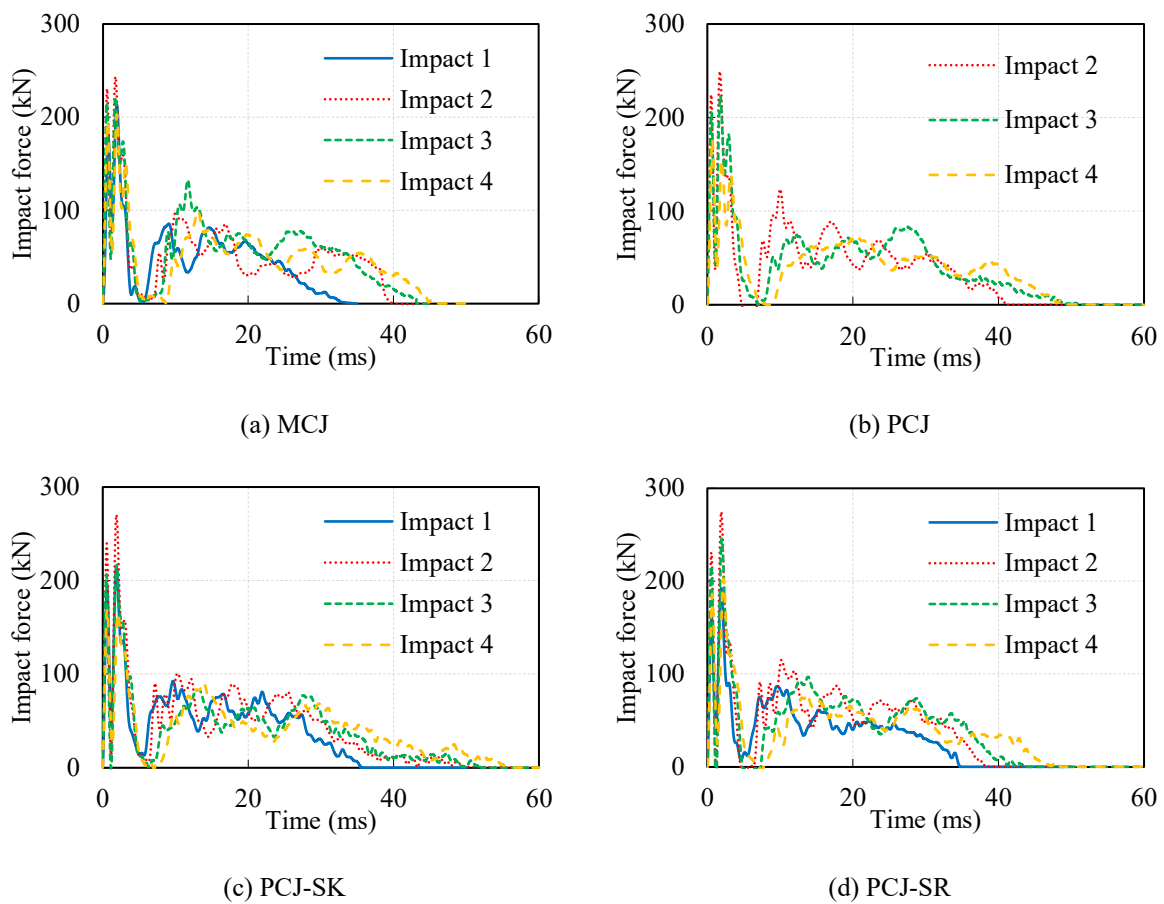
(b) PCJ

(c) PCJ-SK

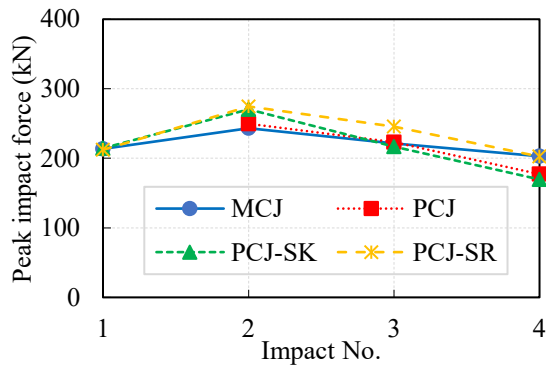(d) PCJ-SR

Fig. 7. Time histories of impact force.
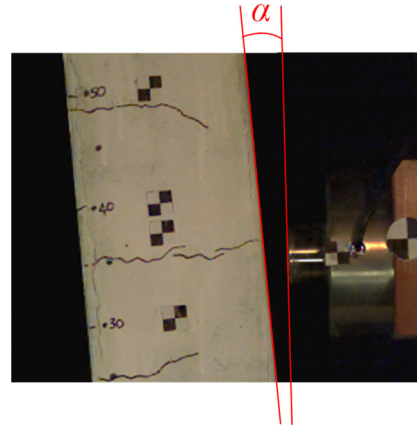
238

Fig. 8. Comparison of peak impact force.

Fig. 9. Inclined angle between load cell and beam in the subsequent impacts.

3.3. Displacement at impact location

The displacement response at the impact location was captured by using the high-speed camera at the tracking point as illustrated in Fig. 5. Fig. 10 shows the time histories of displacement at the impact location. As shown in Fig. 10, the displacements of the specimens under the second impact were larger than those under the first impact as expected because of the increased impact energy and softening of the structure owing to the damage caused by the first impact. The third and fourth impacts with the similar impact energy as the second impact induced even larger displacements. This is because more accumulative impact energy caused more severe damage on the impacted beam and the interface between the PC beam and the CIPC joint area as shown in Fig. 6, which decreased the global stiffness to resist the deformation at the impact location.

(a) MCJ   (b) PCJ
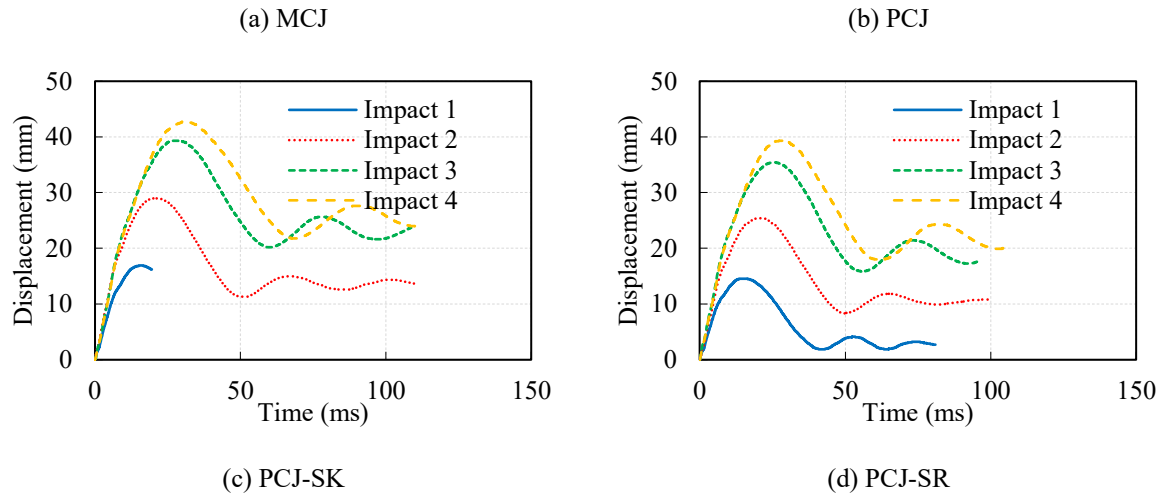
(c) PCJ-SK   (d) PCJ-SR
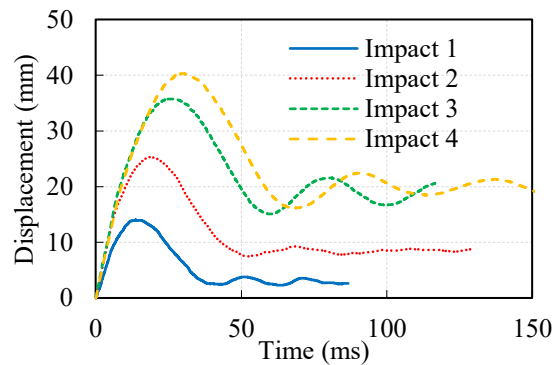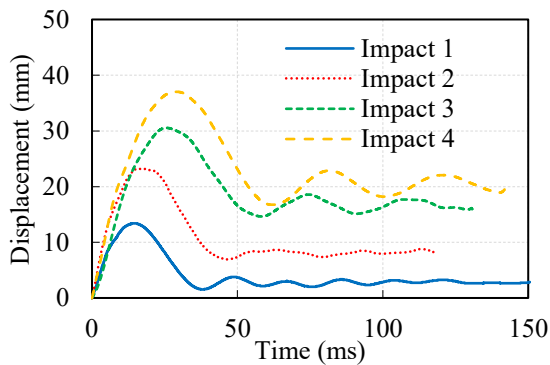
Fig. 10. Time histories of displacement at the impact location.

250   Maximum and residual displacements of specimens under each impact are presented in

251   Table 2 and compared in Fig. 11. The maximum displacements of MCJ, PCJ, and PCJ-SR under

252   the first impact were 13.41 mm, 14.05 mm, and 14.54 mm, which were lower than 16.91 mm

253   of PCJ-SK. From the second impact to the fourth impact, the maximum displacement of MCJ

254   were 23.21mm, 30.56 mm, and 37.02 mm, which were lower than those of the other specimens

255   under the similar impact energy, while the PCJ-SK had the largest maximum displacements of

256   29.07 mm, 39.28mm, and 45.00 mm, respectively. The maximum displacements of PCJ and

257   PCJ-SR were comparable when subjected to the four impacts as shown in Fig. 11(a). The

258   residual displacements of MCJ, PCJ, PCJ-SK, and PCJ-SR under the first impact were 2.87

259   mm, 2.63 mm, 3.16 mm, and 2.68 mm, respectively. With more impact energy imposing on the

260   specimens, the residual displacements increased as shown in Fig. 11(b). After four impacts, the

261   accumulative residual displacements of MCJ, PCJ, PCJ-SK, and PCJ-SR were 46.65 mm 50.85

262   mm, 67.37 mm, and 51.54 mm, respectively, with a difference of 44.16% between MCJ (the

263   smallest residual displacement) and PCJ-SK (the largest residual displacement). This is because

264   the PC joint with shear key (PCJ-SK) experienced a larger rotational response due to the damage

265   along the interface. The PC beam rotated around the shear key under the bending moment

266   induced by impact force. Moreover, the accumulative residual displacement of PCJ (50.88 mm)

267 was comparable to that of PCJ-SR (51.54 mm), with a difference of 1.3%, implying the interface

268 rebar had a very limited effect on the displacement response of PC joint under impact loads
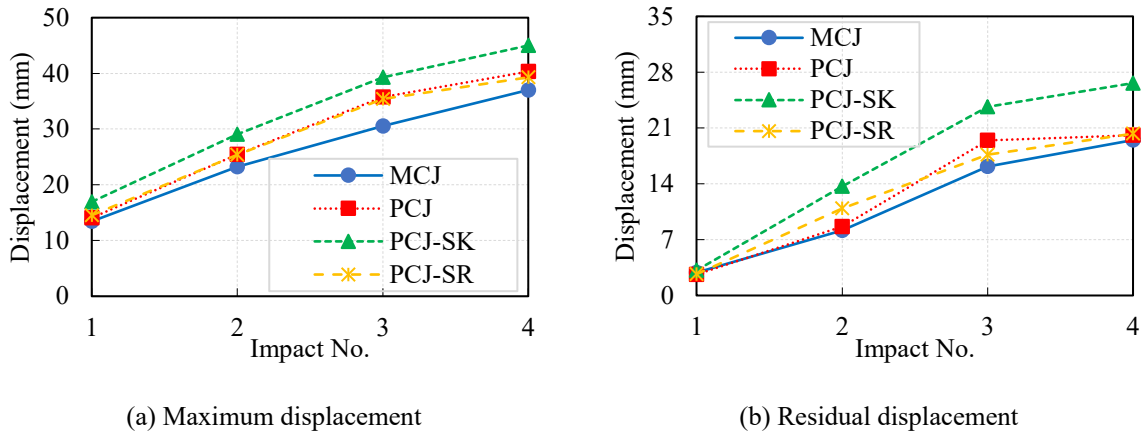
269 acting at the middle of beam.

(a) Maximum displacement   (b) Residual displacement

Fig. 11. Maximum and residual displacements.

3.4. Energy dissipation

271   During impact process, the impact energy imparted to the joint was dissipated in the form

272 of deformation and damage of the specimens. The energy dissipation capacity is an important

273 index to evaluate the impact capacity of beam-column joint. The energy dissipation of the tested

274 specimens depends on the impact force and the displacement at the impact location [36, 44, 45].

275 The relationship between the impact force and displacement at the impact location is presented

276 in Fig. 12. A simplified impact force-displacement curve is presented in Fig. 13 to illustrate the

277 impact energy imposing onto the beam-column joint. At point O (the beginning of impact), the

278 initial input kinetic energy (E_k) that was calculated by impact mass and impact velocity as listed

279 in Table 1 was applied onto the specimen. Point A was the highest point during the first impulse,

280 which corresponded to the peak impact force. Point B was the lowest point at the end of the

281 primary impulse. Then the impact force increased with the increasing of displacement Δ to point

282 C as shown in Fig. 13. The specimen suffered the second impulse from point C owing to the

283 interaction between the specimen and impactor and the displacement increased gradually to

284 Point *D*. At point *D*, the displacement of the impacted beam at the impact location reached the

285 maximum and the velocities of impactor and beam became zero. After reaching the maximum

286 displacement, the impact force decreased gradually to zero and the elastic deformation of the

287 specimen recovered to Point *E*, which caused the release of elastic energy stored in the beam-

288 column joint. Therefore, the dissipated plastic energy (E_p) by the beam-column joint can be

289 calculated by the enclosed area of *OABCDE* as shown in Fig. 13. The energy dissipation

290 capacity of beam-column joint was estimated by using the energy dissipation ratio (E_p/E_k) as
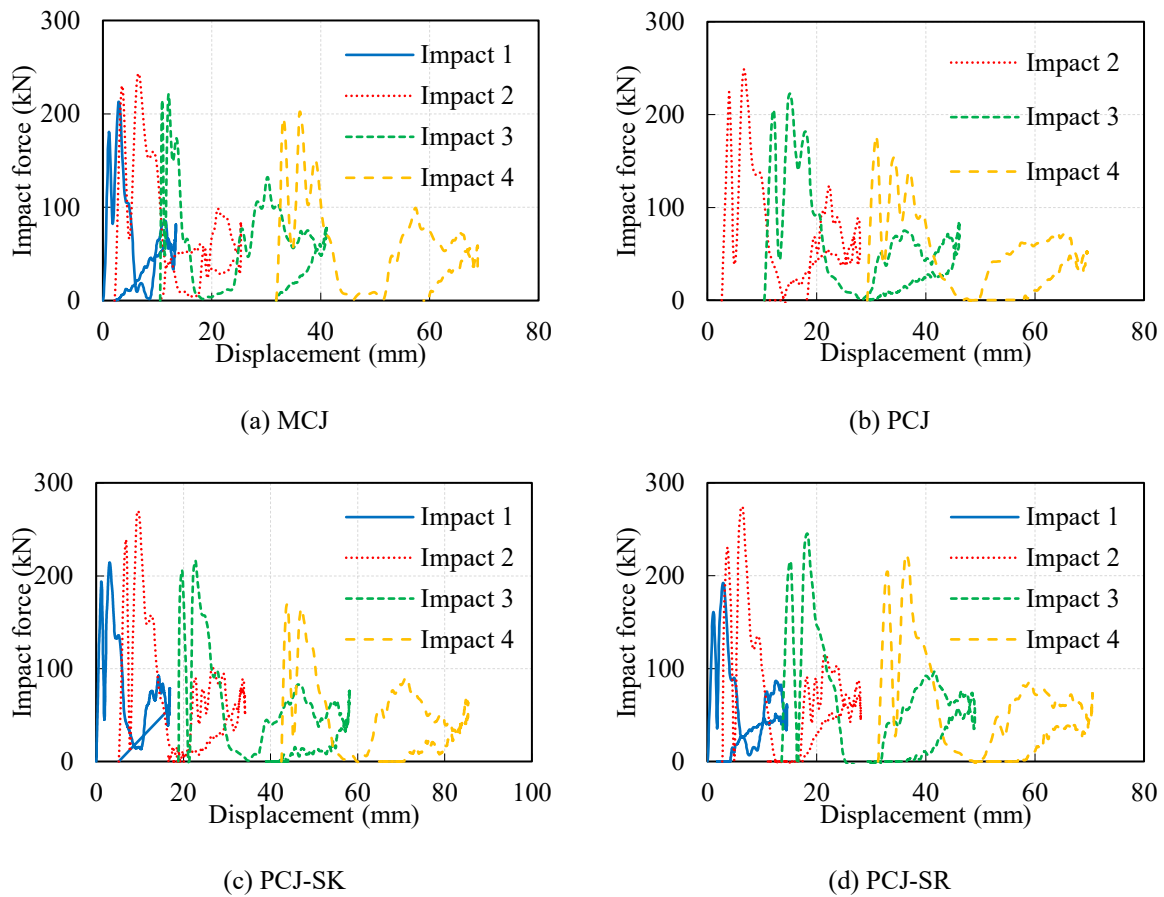
291 shown in Table 2 and Fig. 14.

(a) MCJ

(b) PCJ

(c) PCJ-SK

(d) PCJ-SR

Fig. 12. Relationship between impact force and displacement.

292
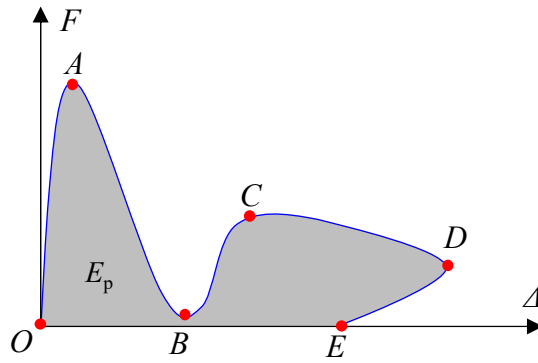
Fig. 13. Illustrative impact force-displacement curve.

As shown in Fig. 14, the dissipated plastic energy of the specimens increased with the impact energy imposing onto the specimens. For example, the dissipated plastic energy of MCJ increased from 604.06 J to 2053.78 J, with an increase of 240%, which indicated that specimen MCJ suffered more severe damage and deformation with the increase of imposed impact energy. Moreover, the energy dissipation ratios (E_p/E_k) of specimen PCJ-SK were 0.59, 0.71, and 0.81 from the first impact to the third impact, which were significantly higher than those of other specimens. Under the fourth impact, specimens MCJ, PCJ, PCJ-SK, and PCJ-SR had similar energy dissipation ratios of 0.72, 0.73, 0.77, and 0.75, respectively, as shown in Fig. 14. It is found that the energy dissipation ratio for all three PC joints decreased from the third impact to the fourth impact (e.g., 0.81 to 0.77 for specimen PCJ-SK) with the similar input energy onto the specimens and larger plastic deformation was observed. This is because the impact force generated in the third impact was larger than that in the fourth impact as shown in Table 2 and Fig. 12. Moreover, the respective accumulative dissipated energy of specimens MCJ, PCJ, PCJ-SK, and PCJ-SR were 5762.92 J, 6297.52 J, 7442.01 J, and 6574.39 J after four impacts. It can be found that the PCJ-SK dissipated more energy than MCJ by 29.14%, PCJ by 18.17%, and PCJ-SR by 13.19%, respectively. Specimen PCJ-SK dissipated energy mainly through the larger deflection of PC beam and severe damage of connection as shown in Fig. 6, which was different from other specimens.
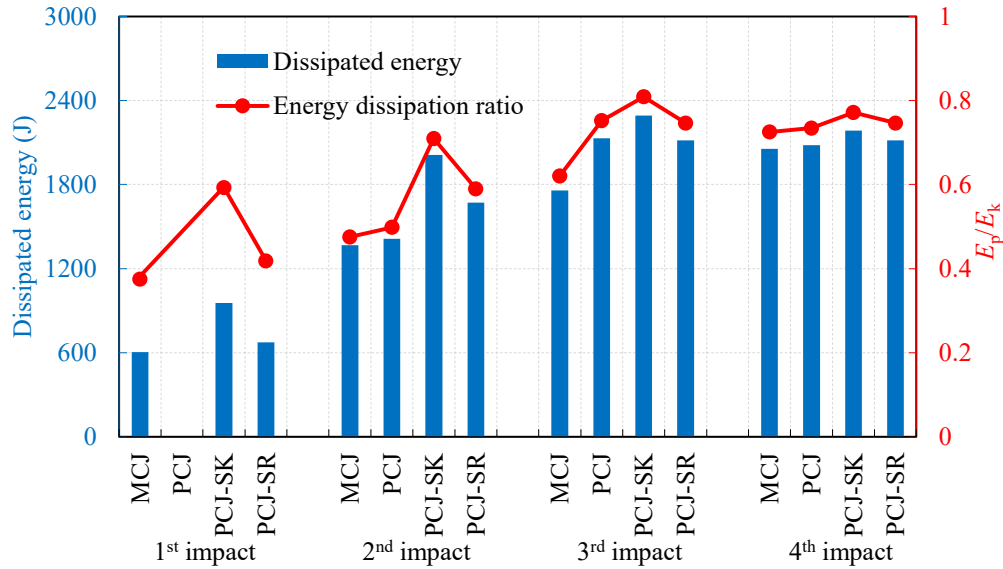
Fig. 14. Comparison of dissipated energy and energy dissipation ratio (E_p/E_k).

3.5. Discussion of the impact performance of different wet connections

As presented in the experimental results of the four beam-column joints, various wet connection configurations led to different impact resistance. The connection configurations had a limited effect on the peak impact force under the first impact because of the same impact energy and contact stiffness at the impact zone as summarized in Ref. [46]. However, in the subsequent impacts, the peak impact force acting on the specimens were different because the joints with different connection configurations experienced different residual deflections of beam and damage after each impact. The residual deflection induced by previous impact could lead to an inclined impact angle between beam and impactor in the subsequent impact and thus reduced the contact area as shown in Fig. 9. Specimen PCJ-SK had the largest accumulative residual deflection of 40.5 mm after three impacts and experienced the lowest peak impact force of 169.38 kN at the fourth impact. Besides, the PC joints PCJ, PCJ-SK, and PCJ-SR dissipated more impact energy than the monolithic joint MCJ as evident by the energy dissipation ratio in Fig. 14. The impact energy was dissipated by experiencing more severe damage at the connections and larger deflections of PC beams. It is worth noting that specimen PCJ-SK dissipated more plastic energy by larger deflection of the PC beam and more severe damage at

interface between PC beam and joint. This is because the impact force would cause larger

deflection of PC beam and larger rotation of the PC beam around joint area in specimen PCJ-

SK. Moreover, the accumulative residual rotations of joints after each impact are presented in

Fig. 15. The monolithic RC joint MCJ presented the minimum accumulative residual rotation

of 0.13 rad after four impacts while specimen PCJ-SK experienced the maximum accumulative

residual rotation of 0.19 rad. It is because the PC beam would rotate around the shear key after

the interface damage between PC beam and CIPC joint area subjected to the bending moment

induced by impact force. The rotation of PCJ-SK mitigated the flexure and shear failure on the

PC beam and the concrete cracks on the PC column as shown in Fig. 6(d). In addition, since the

impact load at the middle of beam could cause flexural-governed damage at the connection area,

the over-reinforced interface rebars at the wet connection induced more severe concrete damage

at the PC beam end close to the joint area (i.e., concrete crushing on the left side and cracking

on the right side) in this study, and thus specimen PCJ-SR experienced slightly larger

accumulative residual rotation than specimen PCJ as shown in Fig. 15.
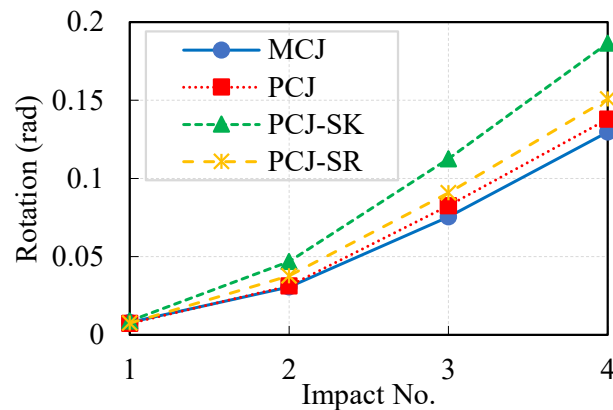
Fig. 15. Accumulative residual rotation of joint under impacts.

In general, the monolithic RC joint MCJ with the best connection integrity presented the

lowest displacement response and dissipated the minimum impact energy. In terms of the PC

joint, specimen PCJ with higher integrity of interface between PC beam and CIPC joint suffered

less severe damage at the PC beam and the joint zone than other PC joints. The PC joint with

shear key (PCJ-SK) experienced the largest rotation and dissipated more impact energy by

351 deflection of the PC beam. The interface rebars that were placed through the interface in

352 specimen PCJ-SR caused more concrete damage on the PC beam close to the joint area as

353 shown in Fig. 6(d), which reduced the impact resistance of specimen and led to a larger

354 displacement than specimen PCJ. In summary, the shear key and interface rebar had a limited

355 contribution to resisting the deformation of PC beam and wet connection when the impact load

356 was applied at the middle of beam. It is worth examining the effects of shear key and interface

357 rebar on the performance of PC joints when the applied impact load is close to the connection

358 area, which can be investigated via numerical simulations.

359 **4. Numerical study**

360 **4.1. Finite element model**

361   Numerical models of beam-column joints with different connections were developed and

362 calibrated by using LS-DYNA as shown in Fig. 16. The constant stress solid element with a

363 single integration point was used for the concrete beam, column, joint, load cell, and weight.

364 Longitudinal rebars and stirrups were simulated by Hughes-Liu beam element with 2×2 Gauss

365 quadrature integration. The load cell in front of the impactor was simulated by the actual

366 dimension to ensure the actual contact area between impactor and beam. The longitudinal rebars

367 and stirrups were embedded into concrete parts by the coupling constrained method [47, 48].

368 The mesh size of 7.5 mm for the numerical model was adopted after conducting a mesh

369 convergence study to obtain reliable results with a reasonable computational cost. A larger mesh

370 size of 50 mm was assigned to the impact mass block for saving computational time. The

371 density of impact mass block was modified to maintain the entire impact mass (including the

372 mass of load cell) as 550 kg. The interfaces between PC and CIPC were simulated by using

373 solid elements with a thickness of 7.5 mm and two elements were employed in the thickness

374 direction. The eroding-single-surface contact was employed for the concrete elements to avoid

375 penetrations after the failure of interface elements. The automatic surface-to-surface contact

376 was defined between the impactor and the beam to obtain the impact force acting on the beam.

377 The column ends were hinge supported by steel plates that can rotate freely. The automatic

378 surface-to-surface contact was also employed between the concrete column and steel plates.

379 The axial force of 60 kN in the test was pre-loaded on the column as shown in Fig. 16 by using

380 dynamic relaxation analysis to reach a steady state. The initial axial load on the column was

381 kept constant in the following impact analysis. The initial impact velocity was assigned to the

382 load cell and weight.
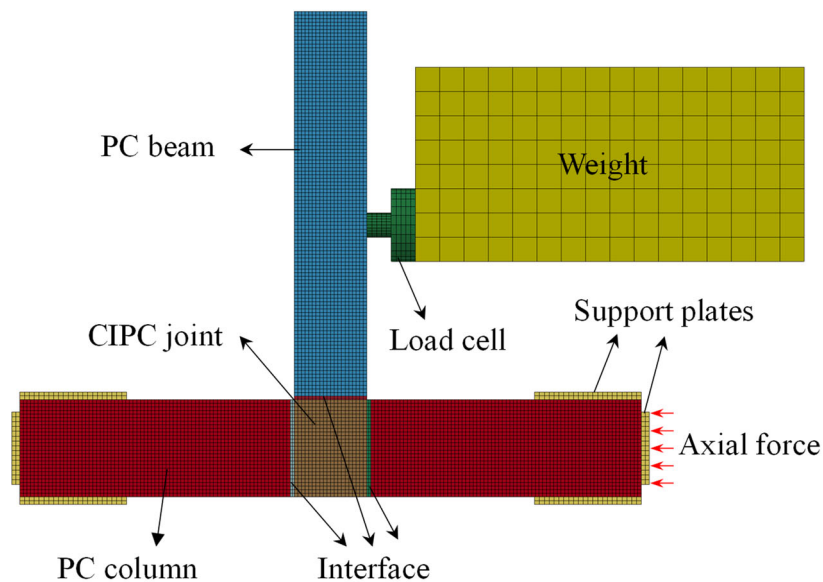
383

384 Fig. 16. Numerical model of beam-column joint.

385 **4.2. Material models**

386 Concrete model (i.e., Karagozian & Case model, Mat_72R3 in LS-DYNA) including

387 strain rate effect, plasticity, and damage softening after failure was employed for the concrete

388 and the interface between PC and CIPC components. Only unconfined compressive strength of

389 concrete material needed be given, and the other model parameters (such as Young's module

390 and tensile strength) were generated automatically by the model using its built-in algorithm.

391 The material erosion criterion with the maximum principal strain of 0.005 was assigned to the

392 interfaces, which was the same as the simulation of PC beam under impact load [20]. The strain

393   rate effect of concrete material was defined by employing the dynamic increase factors (DIFs)

394   for concrete compressive and tensile strength [49]. Moreover, the longitudinal rebars and

395   stirrups were simulated by the elastic-plastic material model (Mat_24 in LS-DYNA). The

396   failure plastic strain for steel was determined as 0.12. When the plastic strain of steel element

397   reaches this value, the element would be deleted from the numerical model. The DIF model for

398   steel material proposed by Malvar [50] was adopted to reflect the strain rate effect of steel. In

399   addition, the elastic material model (Mat_01 in LS-DYNA) was adopted for the load cell,

400   weight block, and steel plates. The detailed material parameters are summarized in Table 3.

401

Table 3. Material parameters used in the numerical model.

Parts	Material model in LS-DYNA	Parameters	Value
Concrete components and interface	CONCRETE_DAMAGE_REL3 (Mat_72R3)	Density	2400 kg/m^3
		Poisson's ratio	0.2
		Compressive strength	64.75 MPa (PC components and interface) 68.34 MPa (CIPC component)
Longitudinal rebar and stirrup	PIECEWISE_LINEAR_PLASTICITY (Mat_24)	Density	7800 kg/m^3
		Young's modulus	200 GPa
		Poisson's ratio	0.3
		Yield strength	500 MPa
Load cell and steel plate	ELASTIC (Mat_01)	Density	7800 kg/m^3
		Young's modulus	200 GPa
		Poisson's ratio	0.3

402   **4.3. Comparison between test and numerical results**

403   Numerical models of monolithic RC and PC beam-column joints were developed and

404   calibrated against the test data using LS-DYNA. The four beam-column joints with different

405   connection configurations under the first impact were simulated, i.e., the impact mass was 550

406   kg and the actual impact velocity for each specimen as listed in Table 1 was employed. The

407   failure modes of joints were compared between numerical and test results in Fig. 17. It can be

408   observed that the numerical concrete damage contours agreed well with the concrete cracks

409   observed in the tests. The concrete cracks at the middle of beam were well predicted in the

410   numerical models. Moreover, the predicted concrete damage on the right side of beam close to

411   the joint area was in good agreement with the observed concrete cracks at the same locations.

412 The interface damage in PC joint was well captured in the numerical model. Besides, the

413 damage mode of shear key in specimen PCJ-SK is shown in Fig. 17, which presented more

414 severe damage on the right side of shear key than the left side.
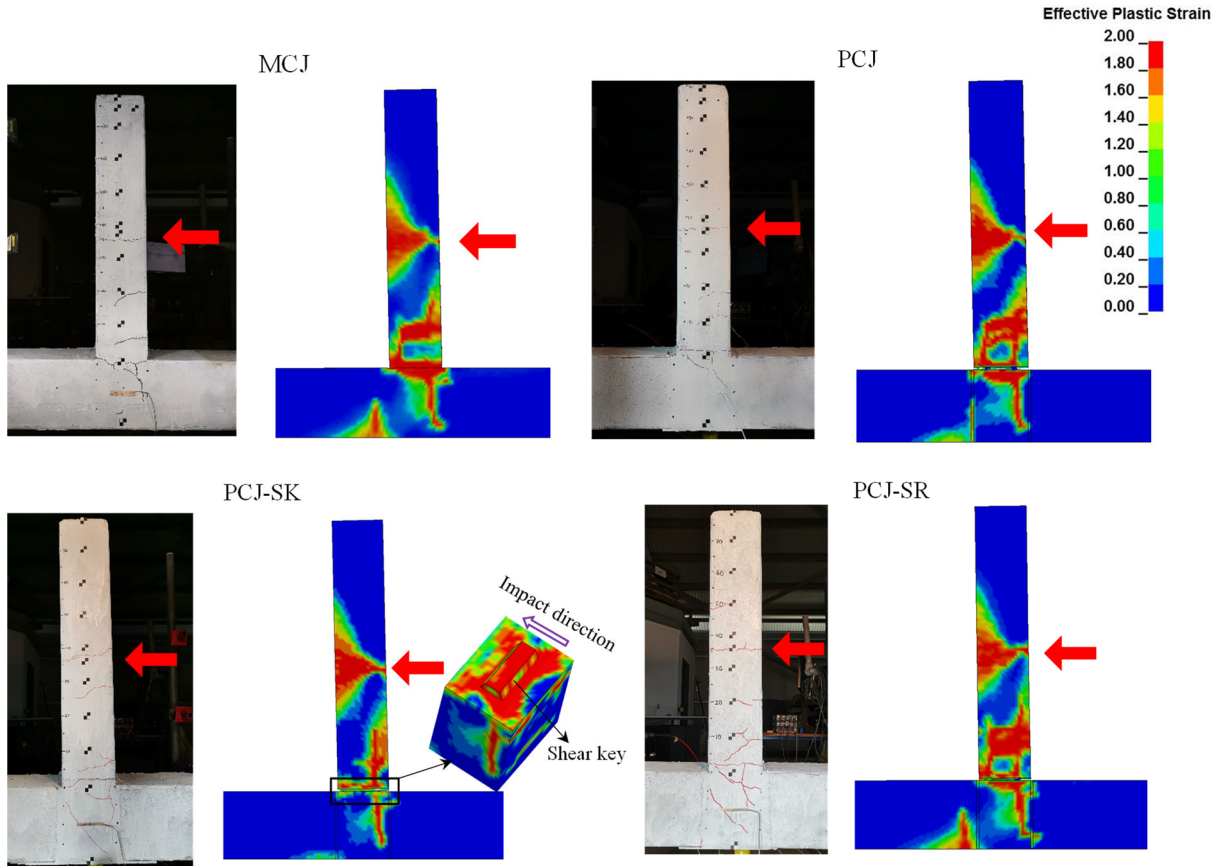

415

416 Fig. 17. Comparison of failure mode between test and numerical results.

417 The predicted time histories of the impact force and displacement were compared with the

418 test results as illustrated in Fig. 18. The numerical peak impact forces of specimens MCJ, PCJ,

419 PCJ-SK, and PCJ-SR under the first impact were 233.76 kN, 224.06 kN, 216.17 kN, and 224.01

420 kN, respectively, which are comparable to the test results as listed in Table 2. It is noted that

421 double peaks appeared in the test results due to the interaction between specimen and impact

422 head, which was affected by the slight deflection of pendulum arm during impact. However,

423 the pendulum arm was not considered in the simulation. In addition, the predicted impact

424 duration by numerical simulation was shorter than the experimental results as shown in Fig.

425 18(a), which might be due to the ideal boundary conditions setting in the numerical models. It

426 should be mentioned that the experimental impact force of specimen PCJ was not recorded and

26

427   could not be compared herein. Moreover, the predicted displacements by the numerical models

428   also agreed well with the experimental displacements as shown in Fig. 18(b).
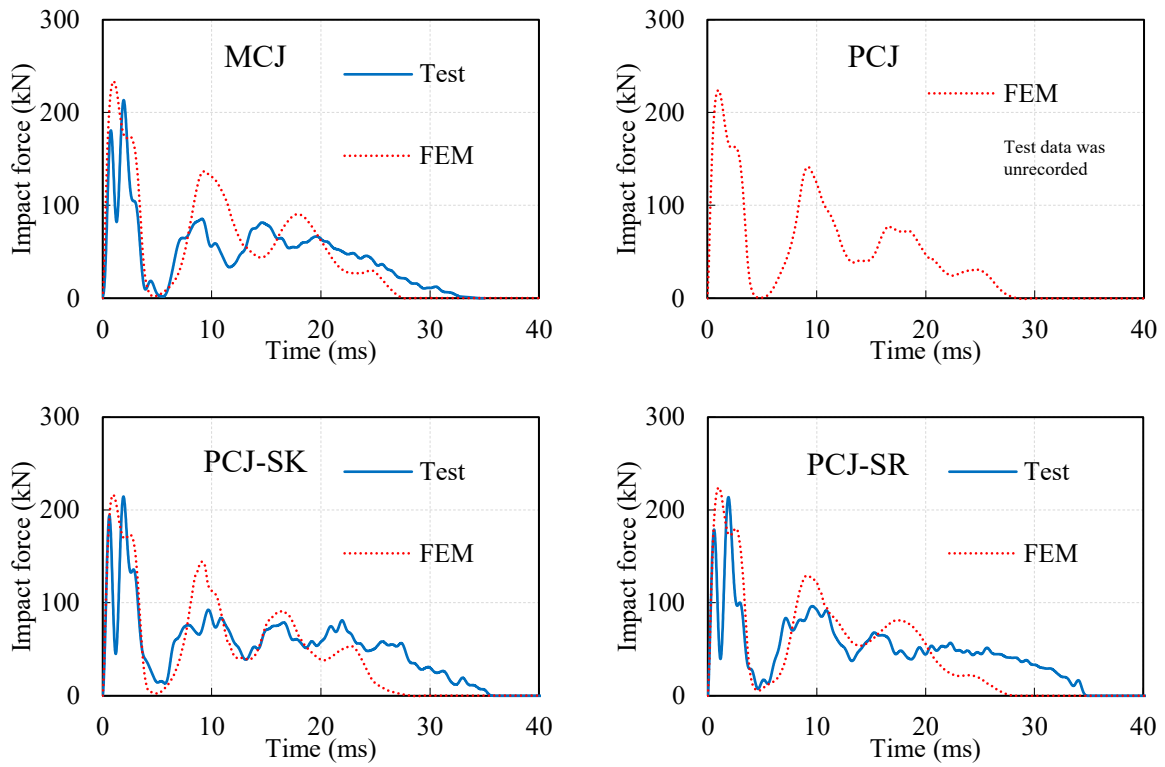
(a) Time history of impact force
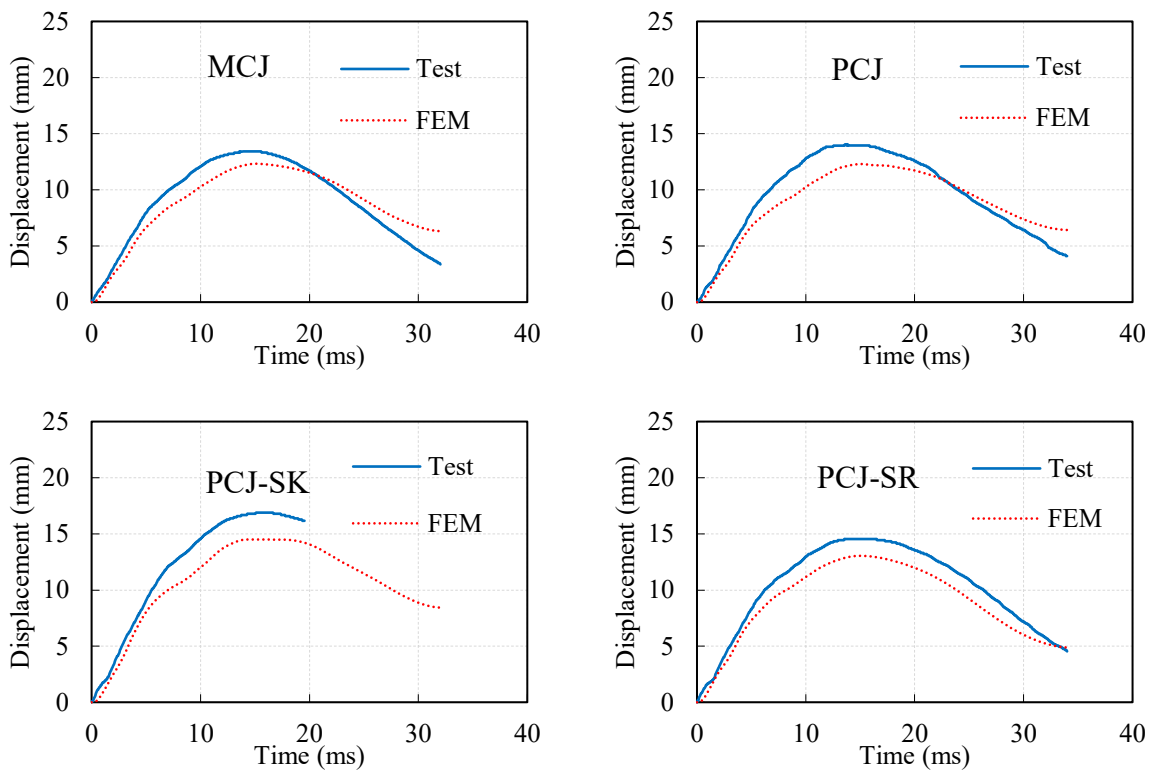
(b) Time history of displacement

Fig. 18. Comparisons of impact force and displacement between test and numerical results.

4.4. Numerical analysis of different wet connections

429

430   In the present impact test, the impact loading was applied at the middle of beam and

431   induced flexural-governed damage at the connections. To further examine the effects of shear

432   key and interface rebars on the impact behaviour of PC joint with wet connections under shear-

433   governed damage, the numerical models of beam-column joint subjected to the impact load

434   close to the connection area were developed as shown in Fig. 19. The distance between the

435   impact location to the joint area was 100 mm. The impact force close to the connection could

436   induce a larger shear action on the connection. To save computational cost, the specimens were

437   impacted only once in the simulation with a large impact energy. The considered impact energy

438   in the simulation was assumed to be equivalent to the accumulated energy from the four impacts

439   in the experimental tests, which was 10.11 kJ (i.e., the sum of 1.61 kJ, 2.83 kJ, 2.83 kJ, and

440   2.83 kJ as listed in Table 1). Accordingly, the impact velocity was assumed as 3.21 m/s and the

441   impact mass as 1962.33 kg by modifying the material density of impact mass block. This

442   modification was made to induce more severe damage in the specimens for clearer comparisons.
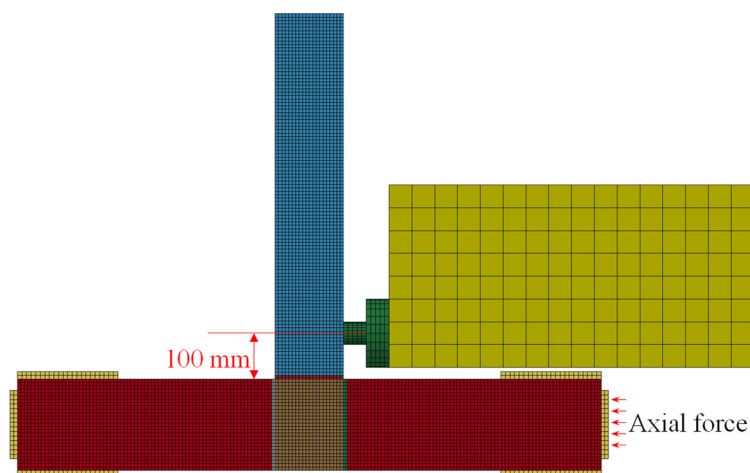

443

444   Fig. 19. Impact at the location close to connection area.

445   Fig. 20 shows the failure modes of shear key and interface rebars at the wet connections.

446   It can be seen from Fig. 20(a) that the shear key at the wet connection experienced obvious

447   shear deformation and severe damage. Besides, the interface rebars exhibited shear dowel

448   deformation on both the left and right sides as illustrated in Fig. 20(b). It is noted that only the

449   interface rebars are presented in Fig. 20(b) for better demonstration. Since the impact force was

450   applied close to the connection area and would induce a larger shear force along the interface,

451   the wet interface between PC beam and CIPC joint experienced a shear-governed damage and

452   the PC beam tended to slip along the interface at the early stage of the impact. The shear action

453   along the interface was resisted by the concrete shear resistance and the dowel resistance of

454   longitudinal rebar [51-53]. With the occurrence of interface damage, shear resistance provided

455   by concrete decreased while the longitudinal rebar at both sides provided more significant shear

456   resistance by the dowel action [54, 55]. For specimen PCJ, the shear force induced by impact

457   load along the interface was mainly resisted by the longitudinal rebar after the failure of

458   interface. However, the PC joints with shear key (PCJ-SK) and interface rebar (PCJ-SR) had

459   additional shear resistances provided by shear key and interface rebar respectively, which

460   reduced the deformation of specimens and thus led to a smaller displacement at the middle of

461   PC beam as shown in Fig. 21(b). Therefore, the shear key and interface rebar were effective to

462   resist the shear failure along the interface when the impact load was applied close to the

463   connection area (i.e., shear-governed damage of connection).

464

(a) Joint with shear key
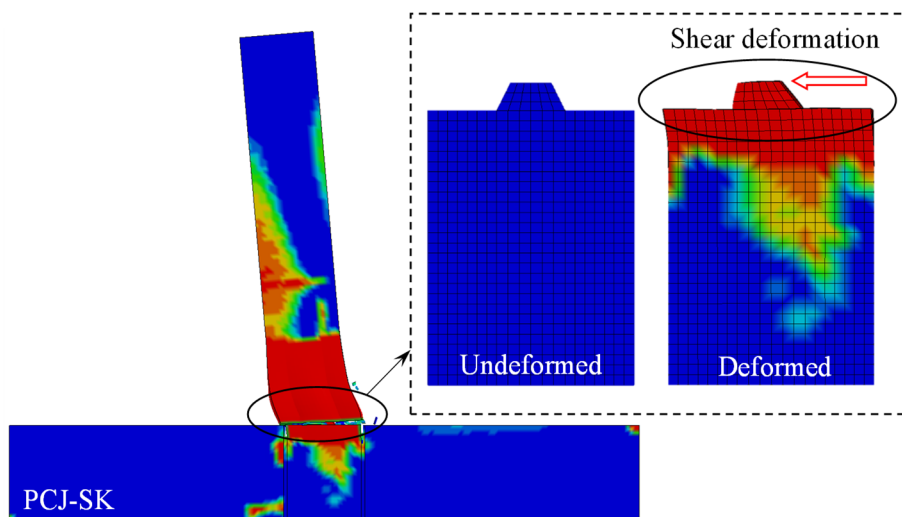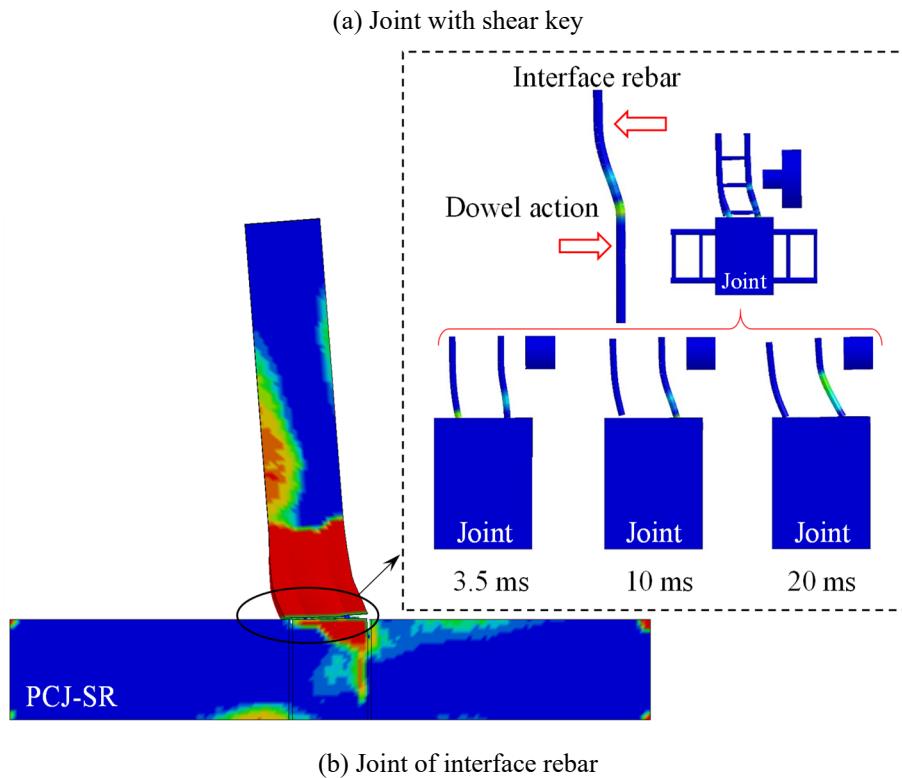
(b) Joint of interface rebar

Fig. 20. Failure modes of the joints with shear key and interface rebar.

Fig. 21 presents the time histories of the impact force at the impact location and displacement at middle of the beam (same monitoring point in the test) of the beam-column joint under the impact close to the connection. The peak impact forces for each specimen were comparable because of the same contact stiffness at the impact zone and impact energy. After the primary impact impulse, a force plateau was observed in each specimen as presented in Fig. 21(a) as impact mass (1962.33 kg) was larger than the mass of specimen, which has been reported in Ref. [47]. The average impact forces at the force plateau stage of specimens MCJ, PCJ, PCJ-SK, and PCJ-SR were 277.62 kN, 163.66 kN, 209.77 kN, and 176.87 kN, respectively. Moreover, the total impact loading durations on specimens MCJ, PCJ, PCJ-SK, and PCJ-SR were 43.9 ms, 57.9 ms, 53.6 ms, and 56.2 ms, respectively. The impact force acting on specimen MCJ presented the largest plateau impact force and the shortest impact duration, indicting the best integrity of monolithic RC joint. This is consistent with the conclusion that the larger global resistance of specimen under impact load could lead to a higher force plateau and a shorter duration as reported in Refs. [29, 56]. For the PC joints, the specimens with shear key (PCJ-

483   SK) and interface rebar (PCJ-SR) had a larger plateau impact force and a shorter impact

484   duration than those in specimen PCJ. It is because that the shear key and interface rebar

485   improved the shear resistance of wet connection under impact load.

486   The displacement at the middle of beam is illustrated in Fig. 21(b). The maximum

487   displacements of specimens MCJ, PCJ, PCJ-SK, and PCJ-SR were 51.07 mm, 87.12 mm, 68.11

488   mm, and 75.18 mm, respectively, while the residual displacements of the specimens were, 41.62

489   mm, 73.37 mm, 58.79 mm, and 60.75 mm, respectively. Specimen MCJ had the lowest

490   displacement due to the monolithic connection between beam and column. The residual

491   displacement of PCJ was 24.79% and 20.77% larger than the displacement of specimens PCJ-

492   SK and PCJ-SR, respectively, which indicated that the shear key and interface rebars could

493   provide a better capacity to resist the shear-governed damage induced by impact load, as

494   compared with PCJ. In addition, specimen PCJ-SK exhibited a slightly lower residual

495   displacement than specimen PCJ-SR, indicating that the shear key was slightly more effective

496   than the interface rebars against the shear action at the wet connection. These results indicate

497   that if the response is governed by shear mode, shear key at the interface is the most effective

498   in mitigating the response, but it is ineffective and even has some adverse effect when the

499   response is governed by flexural mode as demonstrated above. Therefore, to be able to mitigate

500   both shear and flexural response, modified design that can provide both shear and bending

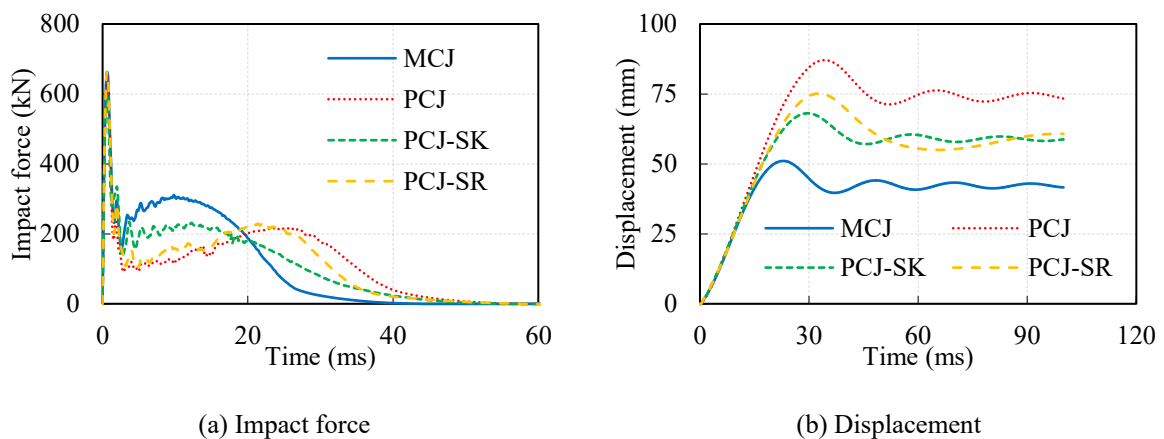501   resistance is needed. This, however, will be a topic of next research.

(a) Impact force   (b) Displacement

5. Conclusions

This study investigated the dynamic response of monolithic RC and PC beam-column joints with different connection configurations. The failure mode, impact force, displacement at impact location, and energy dissipation were analysed and compared. In addition, numerical models of beam-column joints were developed by using LS-DYNA to further examine the dynamic behaviour of joints with different wet connection configurations and subjected to impact at different locations. The main conclusions are summarized as follows.

(1) When the impact loads were applied at the middle of beam in the test as shown in Fig. 5, the monolithic RC joint MCJ experienced less concrete damage at the joint area but more flexural and shear concrete cracks on the beam. The PC joints experienced more severe interface damage between beam and joint area. The monolithic RC joint showed better connection integrity than PC joints with less residual rotation. Using the shear key (PCJ-SK) and interface rebar (PCJ-SR) did not enhance the impact resistance of the joint when response was governed by flexural mode. However, specimen PCJ-SK showed fewer concrete cracks on the PC beam as the PC beam rotated around the shear key after the damage of interface.

(2) When the impact loads were applied near the connection (i.e., 100 mm from the connection area in the numerical study) as shown in Fig. 19, the shear key and interface rebars demonstrated the effectiveness in resisting the shear-governed response of the wet connection, indicating the shear key and interface rebars were beneficial for PC joints to resist shear-governed response but not effective in resisting flexural-governed response induced by impact load.

In general, various wet connection configurations for the concrete beam-column joints under impact load could lead to different dynamic responses and damage modes. The impact location that causes different combinations of bending moment and shear force acting at the

32

526   joint should be considered when designing the beam-column joint with wet connection.

532 **References**

533 [1]. Lu, C., Dong, B., Pan, J., Shan, Q., Hanif, A., and Yin, W., *An investigation on the behavior*
534   *of a new connection for precast structures under reverse cyclic loading.* Engineering
535   Structures, 2018. 169: 131-140.
536 [2]. Zhang, Z.-Y., Ding, R., Nie, X., and Fan, J.-S., *Seismic performance of a novel interior*
537   *precast concrete beam-column joint using ultra-high performance concrete.* Engineering
538   Structures, 2020. 222: 111145.
539 [3]. Kurama, Y.C., Sritharan, S., Fleischman, R.B., Restrepo, J.I., Henry, R.S., Cleland, N.M.,
540   Ghosh, S.K., and Bonelli, P., *Seismic-resistant precast concrete structures: state of the art.*
541   Journal of Structural Engineering, 2018. 144(4): 03118001.
542 [4]. Joint ACI-ASCE Committee 550, *Design guide for connections in precast jointed systems.*
543   2013: USA.
544 [5]. Joint ACI-ASCE Committee 550, *Guide to emulating cast-in-place detailing for seismic*
545   *design of precast concrete structures.* 2009: USA.
546 [6]. Gou, S., Ding, R., Fan, J., Nie, X., and Zhang, J., *Seismic performance of a novel precast*
547   *concrete beam-column connection using low-shrinkage engineered cementitious*
548   *composites.* Construction and Building Materials, 2018. 192: 643-656.
549 [7]. Eom, T.S., Park, H.G., Hwang, H.J., and Kang, S.M., *Plastic hinge relocation methods for*
550   *emulative pc beam-column connections.* Journal of Structural Engineering, 2016. 142(2):
551   13.
552 [8]. Wang, X., Li, L.-Z., Deng, B.-Y., Zhang, Z., and Jia, L., *Experimental study on seismic*
553   *behavior of prefabricated RC frame joints with T-shaped columns.* Engineering Structures,
554   2021. 233: 111912.
555 [9]. Liu, H., Yan, Q., and Du, X., *Seismic performance comparison between precast beam joints*
556   *and cast-in-place beam joints.* Advances in Structural Engineering, 2017. 20(9): 1299-
557   1314.
558 [10]. Kang, S. and Tan, K., *Progressive collapse resistance of precast concrete frames with*
559   *discontinuous reinforcement in the joint.* Journal of Structural Engineering, 2017. 143(9):
560   04017090.
561 [11]. Lee, H.-J., Chen, H.-C., and Syu, J.-H., *Seismic performance of emulative precast concrete*
562   *beam–column connections with alternative reinforcing details.* Advances in Structural
563   Engineering, 2017. 20(12): 1793-1806.
564 [12]. Yang, H., Guo, Z., Yin, H., Guan, D., and Yang, S., *Development and testing of precast*
565   *concrete beam-to-column connections with high-strength hooked bars under cyclic loading.*

566   Advances in Structural Engineering, 2019. 22(14): 3042-3054.

567 [13]. Gou, S., Ding, R., Fan, J., Nie, X., and Zhang, J., *Experimental study on seismic*
568   *performance of precast LSECC/RC composite joints with U-shaped LSECC beam shells.*
569   Engineering Structures, 2019. 189: 618-634.

570 [14]. Chen, S., Yan, W., and Gao, J., *Experimental investigation on the seismic performance of*
571   *large-scale interior beam-column joints with composite slab.* Advances in Structural
572   Engineering, 2012. 15(7): 1227-1237.

573 [15]. Yan, X., Wang, S., Huang, C., Qi, A., and Hong, C., *Experimental study of a new precast*
574   *prestressed concrete joint.* Applied Sciences, 2018. 8(10): 1871.

575 [16]. International Federation for Structural Concrete, *Seismic design of precast concrete*
576   *building structures.* 2003, International Federation for Structural Concrete: Lausanne,
577   Switzerland.

578 [17]. Ghayeb, H.H., Razak, A.H., and Sulong, R.N.H., *Seismic performance of innovative*
579   *hybrid precast reinforced concrete beam-to-column connections.* Engineering Structures,
580   2020. 202: 109886.

581 [18]. Kang, S. and Tan, K., *Behaviour of precast concrete beam–column sub-assemblages*
582   *subject to column removal.* Engineering Structures, 2015. 93: 85-96.

583 [19]. Kang, S. and Tan, K., *Robustness assessment of exterior precast concrete frames under*
584   *column removal scenarios.* Journal of Structural Engineering, 2016. 142(12): 04016131.

585 [20]. Li, H., Chen, W., and Hao, H., *Dynamic response of precast concrete beam with wet*
586   *connection subjected to impact loads.* Engineering Structures, 2019. 191: 247-263.

587 [21]. Guan, D., Jiang, C., Guo, Z., and Ge, H., *Development and seismic behavior of precast*
588   *concrete beam-to-column connections.* Journal of Earthquake Engineering, 2018. 22(2):
589   234-256.

590 [22]. International Federation for Structural Concrete, *Model code for concrete structures.* 2013:
591   Lausanne, Switzerland.

592 [23]. Wang, H., Yang, B., Chen, K., and Elchalakani, M., *Parametric analysis and simplified*
593   *approach for steel-framed subassemblies with reverse channel connection under falling-*
594   *debris impact.* Engineering Structures, 2020. 225: 111263.

595 [24]. Wang, H., Tan, K.H., and Yang, B., *Experimental tests of steel frames with different beam-*
596   *column connections under falling debris impact.* Journal of Structural Engineering, 2020.
597   146(1): 04019183.

598 [25]. Fujikake, K., Li, B., and Soeun, S., *Impact response of reinforced concrete beam and its*
599   *analytical evaluation.* Journal of Structural Engineering, 2009. 135(8): 938-950.

600 [26]. Pham, T.M., Hao, Y., and Hao, H., *Sensitivity of impact behaviour of RC beams to contact*
601   *stiffness.* International Journal of Impact Engineering, 2018. 112: 155-164.

602 [27]. Yan, Q., Sun, B., Liu, X., and Wu, J., *The effect of assembling location on the performance*
603   *of precast concrete beam under impact load.* Advances in Structural Engineering, 2018.
604   21(8): 1211-1222.

605 [28]. Hwang, H.-J., Yang, F., Zang, L., Baek, J.-W., and Ma, G., *Effect of impact load on splice*
606   *length of reinforcing bars.* International Journal of Concrete Structures and Materials, 2020.
607   14(1): 40.

608 [29]. Li, H., Chen, W., Pham, T.M., and Hao, H., *Analytical and numerical studies on impact*
609   *force profile of RC beam under drop weight impact.* International Journal of Impact
610   Engineering, 2021. 147: 103743.

611 [30]. Pham, T.M., Chen, W., Elchalakani, M., Karrech, A., and Hao, H., *Experimental*
612   *investigation on lightweight rubberized concrete beams strengthened with BFRP sheets*
613   *subjected to impact loads.* Engineering Structures, 2020. 205: 110095.

614 [31]. Pham, T.M. and Hao, H., *Plastic hinges and inertia forces in RC beams under impact*
615   *loads.* International Journal of Impact Engineering, 2017. 103: 1-11.

616 [32]. Cotsovos, D.M., *A simplified approach for assessing the load-carrying capacity of*
617 *reinforced concrete beams under concentrated load applied at high rates.* International
618 Journal of Impact Engineering, 2010. 37(8): 907-917.
619 [33]. Vlassis, A.G., Izzuddin, B.A., Elghazouli, A.Y., and Nethercot, D.A., *Progressive collapse*
620 *of multi-storey buildings due to failed floor impact.* Engineering Structures, 2009. 31(7):
621 1522-1534.
622 [34]. Kiakojouri, F., Biagi, V.D., Chiaia, B., and Sheidaii, M.R., *Progressive collapse of framed*
623 *building structures: Current knowledge and future prospects.* Engineering Structures, 2020.
624 206: 110061.
625 [35]. Grimsmo, E.L., Clausen, A.H., Langseth, M., and Aalberg, A., *An experimental study of*
626 *static and dynamic behaviour of bolted end-plate joints of steel.* International Journal of
627 Impact Engineering, 2015. 85: 132-145.
628 [36]. Chen, Y., Huo, J., Chen, W., Hao, H., and Elghazouli, A.Y., *Experimental and numerical*
629 *assessment of welded steel beam-column connections under impact loading.* Journal of
630 Constructional Steel Research, 2020. 175: 106368.
631 [37]. Wang, H., Huo, J., Liu, Y., Elchalakani, M., and Zhu, Z., *Dynamic performance of*
632 *composite beam-column connections subjected to impact loadings.* Journal of
633 Constructional Steel Research, 2021. 178: 106498.
634 [38]. Ngo, T.T., Pham, T.M., and Hao, H., *Ductile and dry exterior joints using CFRP bolts for*
635 *moment-resisting frames.* Structures, 2020. 28: 668-684.
636 [39]. Ngo, T.T., Pham, T.M., Hao, H., Chen, W., and Elchalakani, M., *Performance of*
637 *monolithic and dry joints with GFRP bolts reinforced with different fibres and GFRP bars*
638 *under impact loading.* Engineering Structures, 2021. 240: 112341.
639 [40]. ACI Committee 318, *Building code requirements for structural concrete.* 2019: USA.
640 [41]. Joint ACI-ASCE Committee 352, *Recommendations for design of beam-column*
641 *connections in monolithic reinforced concrete structures.* 2002: USA.
642 [42]. Pham, T.M. and Hao, H., *Effect of the plastic hinge and boundary conditions on the impact*
643 *behavior of reinforced concrete beams.* International Journal of Impact Engineering, 2017.
644 102: 74-85.
645 [43]. Li, H., Chen, W., and Hao, H., *Influence of drop weight geometry and interlayer on impact*
646 *behavior of RC beams.* International Journal of Impact Engineering, 2019. 131: 222-237.
647 [44]. Pham, T.M., Zhang, X., Elchalakani, M., Karrech, A., Hao, H., and Ryan, A., *Dynamic*
648 *response of rubberized concrete columns with and without FRP confinement subjected to*
649 *lateral impact.* Construction and Building Materials, 2018. 186: 207-218.
650 [45]. Xian, W., Wang, W.-D., Wang, R., Chen, W., and Hao, H., *Dynamic response of steel-*
651 *reinforced concrete-filled circular steel tubular members under lateral impact loads.* Thin-
652 Walled Structures, 2020. 151: 106736.
653 [46]. Pham, T.M., Chen, W., and Hao, H., *Review on impact response of reinforced concrete*
654 *beams: Contemporary understanding and unsolved problems.* Advances in Structural
655 Engineering, 2021: 1-22.
656 [47]. Li, H., Chen, W., and Hao, H., *Factors influencing impact force profile and measurement*
657 *accuracy in drop weight impact tests.* International Journal of Impact Engineering, 2020.
658 145: 103688.
659 [48]. Huang, Z., Chen, W., Hao, H., Chen, Z., Pham, T.M., Tran, T.T., and Elchalakani, M.,
660 *Shear behaviour of ambient cured geopolymer concrete beams reinforced with BFRP bars*
661 *under static and impact loads.* Engineering Structures, 2021. 231: 111730.
662 [49]. Hao, Y. and Hao, H., *Influence of the concrete DIF model on the numerical predictions of*
663 *RC wall responses to blast loadings.* Engineering Structures, 2014. 73: 24-38.
664 [50]. Malvar, L.J., *Review of static and dynamic properties of steel reinforcing bars.* Materials
665 Journal, 1998. 95(5): 609-616.

666 [51]. Randl, N., *Design recommendations for interface shear transfer in fib Model Code 2010.*
667 Structural Concrete, 2013. 14(3): 230-241.
668 [52]. Santos, P.M.D. and Júlio, E.N.B.S., *Interface shear transfer on composite concrete*
669 *members.* ACI Structural Journal, 2014. 111(1): 113-121.
670 [53]. Santos, P.M.D. and Júlio, E.N.B.S., *A state-of-the-art review on shear-friction.*
671 Engineering Structures, 2012. 45(Supplement C): 435-448.
672 [54]. Ince, R., Yalcin, E., and Arslan, A., *Size-dependent response of dowel action in R.C.*
673 *members.* Engineering Structures, 2007. 29(6): 955-961.
674 [55]. Jeong, E., Lee, K.-C., Lee, S.-C., Seo, J., and Lee, J., *Prediction of dowel action against*
675 *concrete core without consideration of transverse reinforcement.* Journal of Structural
676 Engineering, 2020. 146(12): 04020279.
677 [56]. Zhao, D., Yi, W., and Kunnath, S.K., *Shear mechanisms in reinforced concrete beams*
678 *under impact loading.* Journal of Structural Engineering, 2017. 143(9): 04017089.
679